Available online at www.sciencedirect.com

ScienceDirect

Geochimica et Cosmochimica Acta 218 (2017) 167–200

Geochimica et Cosmochimica Acta

www.elsevier.com/locate/gca

The mineralogy and petrology of I-type cosmic spherules: Implications for their sources, origins and identification in sedimentary rocks

Matthew J. Genge [a,b,*], Bridie Davies [a], Martin D. Suttle [a,b], Matthias van Ginneken [c], Andrew G. Tomkins [d]

[a] Department of Earth Science and Engineering, Imperial College London, Exhibition Road, London 2AZ 11BW, UK
[b] Earth Sciences Department, The Natural History Museum, Cromwell Road, London SW7 2BW, UK
[c] Earth System Science, Vrije Universiteit Brussel, Pleinlaan, 2B-1050 Brussel, Belgium
[d] School of Earth, Atmosphere & Environment, Monash University, Melbourne, Victoria 3800, Australia

Received 24 May 2016; accepted in revised form 31 August 2017; available online 9 September 2017

Abstract

I-type cosmic spherules are micrometeorites that formed by melting during atmospheric entry and consist mainly of iron oxides and FeNi metal. I-types are important because they can readily be recovered from sedimentary rocks allowing study of solar system events over geological time. We report the results of a study of the mineralogy and petrology of 88 I-type cosmic spherules recovered from Antarctica in order to evaluate how they formed and evolved during atmospheric entry, to constrain the nature of their precursors and to establish rigorous criteria by which they may be conclusively identified within sediments and sedimentary rocks. Two textural types of I-type cosmic spherule are recognised: (1) metal bead-bearing (MET) spherules dominated by Ni-poor (<1.5 wt%) wüstite and FeNi metal (10–95 wt% Ni) with minor magnetite, and (2) metal bead-free (OX) spherules dominated by Ni-rich wüstite (0.5–22.5 wt%) and magnetite. Two varieties of OX spherule are distinguished, magnetite-poor dendritic spherules and magnetite-rich coarse spherules. Six OXMET particles having features of both MET and OX spherules were also observed. The wüstite to magnetite ratios and metal contents of the studied particles testify to their formation by melting of extraterrestrial FeNi grains during progressive oxidation in the atmosphere. Precursors are suggested to be mainly kamacite and rare taenite grains. Vesicle formation within metal beads and extrusion of metallic liquid into surrounding wüstite grain boundaries suggests an evaporated iron sulphide or carbide component within at least 23% of particles. The Ni/Co ratios of metal vary from 14 to >100 and suggest that metal from H-group ordinary, CM, CR and iron meteorites may form the majority of particles. Oxidation during entry heating increases in the series MET < magnetite-poor OX < magnetite-rich OX spherules owing to differences in particle size, entry angle and velocity. Magnetite-poor OX spherules are shown to form by crystallisation of non-stoichiometric wüstite at the liquidus followed by sub-solidus decomposition to magnetite, whilst in magnetite-rich OX spherules magnetite crystallises directly at the liquidus. Magnetite rims found on most particles are suggested to form by oxidation during sub-solidus flight. The separation of metal beads due to deceleration is proposed to have been minor with most OX spherules shown to have been in equilibrium with metal beads containing >80 wt% Ni comprising a particle mass fraction of <0.2. Non-equilibrium effects in the exchange of Ni between wüstite and metal, and magnetite and wüstite are suggested as proxies for the rate of oxidation and cooling rate respectively. Variations in magnetite and wüstite crystal sizes are also suggested to relate to cooling rate allowing relative entry angle of particles to be evaluated. The formation of secondary metal in the form of sub-micron Ni-rich or Pt-group nuggets and as symplectite with magnetite was also identified and suggested to occur largely due to the exsolution of metallic alloys during

* Corresponding author at: Department of Earth Science and Engineering, Imperial College London, Exhibition Road, London SW7 2AZ, UK.

https://doi.org/10.1016/j.gca.2017.09.004

decomposition of non-stoichiometric wüstite. Weathering is restricted to replacement of metal by iron hydroxides. The following criteria are recommended for the conclusive identification of I-type spherules within sediments and sedimentary rocks: (i) spherical particle morphologies, (ii) dendritic crystal morphologies, (iii) the presence of wüstite and magnetite, (iv) Ni-bearing wüstite and magnetite, and (v) the presence of relict FeNi metal.

Keywords: Micrometeorite; Antarctica; Cosmic spherules; I-type

1. INTRODUCTION

Micrometeorites are extraterrestrial dust particles <2 mm in diameter that survive atmospheric entry to be collected from the Earth's surface (Genge et al., 2008). These particles are captured by the Earth from the inner Solar System's Zodiacal cloud and provide samples of small bodies including asteroids and comets. Micrometeorites can, therefore, provide information on the origin and evolution of asteroids and comets (e.g. Genge et al., 1997; Genge, 2008; Gounelle et al., 2009; Noguchi et al., 2015) and variations in the dust flux arriving at Earth due to collisional and dynamic disturbances (e.g. Taylor and Brownlee, 1991; Heck et al., 2010; Dredge et al., 2010).

Those micrometeorites that have experienced significant melting during atmospheric entry form sub-spherical particles known as cosmic spherules (Brownlee, 1985). The spherical shapes of these particles and their characteristic surface textures make them readily identifiable amongst samples of terrestrial sediment under a binocular microscope. Cosmic spherules are thus a useful proxy for total micrometeorite abundance (Maurette et al., 1991; Taylor and Brownlee, 1991; Taylor et al., 2000). Cosmic spherules are divided into three classes: (1) S-type cosmic spherules dominated by silicates, (2) I-types dominated by iron oxides and metal, and (3) G-type spherules, which are an intermediate class (e.g. Brownlee, 1985; Taylor et al., 2000; Genge et al., 2008). Iron-type spherules are particularly important since they can be collected readily by magnetic separation allowing them to be concentrated in separates (Dredge et al., 2010; Voldman et al., 2013; Tomkins et al., 2016). The mineralogy of I-types, which is dominated by the iron oxides magnetite and wüstite (Brownlee et al., 1984; Brownlee, 1985; Genge et al., 2008), also makes them resistant to chemical alteration allowing preservation in the geological record (Taylor and Brownlee, 1991; Davidson et al., 2007; Dredge et al., 2010; Onoue et al., 2011; Voldman et al., 2013). The recent discovery of I-type spherules in 2.7 Ga Archean limestones, in particular, demonstrates their ability to record the extraterrestrial dust flux over most of Earth history (Tomkins et al., 2016). Furthermore, given their mineralogy and mechanisms of formation, it has been suggested that these fossil I-type spherules may be able to provide insights into the chemical evolution of the Earth's upper atmosphere (Tomkins et al., 2016).

Although I-type cosmic spherules are readily collected from modern and ancient sediments, their positive identification as extraterrestrial dust is fraught with difficulty. Within modern sediments anthropogenic magnetic dust is abundant and includes iron-rich oxide particles (Anselmo, 2007; Larsen, 2016). Within ancient sediments from the geological column magnetite spheres can be diagenetic or detrital in origin (Suk et al., 1990). There have also been few studies that have focused specifically on the petrology and mineralogy of I-type spherules, largely because of their relatively low abundance within MM collections (Maurette et al., 1991; Taylor et al., 2000; Rochette et al., 2008; Parashar et al., 2010), and consequently little quantitative textural, mineralogical and chemical data on I-types is available to allow meaningful comparisons and positive identification.

The occurrence of FeNi metal droplets mantled by iron oxide within many particles has led to a consensus that the precursors of I-types, prior to entry into the Earth's atmosphere, were metal grains (Yada et al., 1996; Herzog et al., 1999; Engrand et al., 2005; Genge, 2016). The oxygen isotope compositions of I-types are terrestrial and reveal that they acquire their oxygen during atmospheric entry heating (Engrand et al., 2005). Iron, nickel and oxygen isotope compositions of large I-types furthermore indicate significant evaporation occurs during heating (~55–85% by mass) whilst oxidation is occurring (Herzog et al., 1999; Engrand et al., 2005). Oxidation is also known to cause increases in the Ni-content of metal beads found in some spherules (Brownlee and Bates, 1983) and produce Pt-group metal nuggets through oxidation of metal (Brownlee and Bates, 1983; Bonte et al., 1987; Rudraswami et al., 2011). Studies of the bulk composition and Fe, Ni and Cr isotope compositions of I-types suggest they have a chondritic source (Herzog et al., 1999), however, their exact parent bodies remain uncertain. The oxidation of metal during heating in the atmosphere, together with significant evaporative mass loss (Herzog et al., 1999; Engrand et al., 2005) make the identification of the exact nature of their precursors difficult to determine and thus complicate comparisons with meteorite metal phases that could allow the identification of parent bodies.

Previous studies have noted that I-types vary in mineralogy from wüstite to magnetite-rich (Brownlee and Bates, 1983; Engrand et al., 2005) and some exhibit magnetite rims, metal-beads (Engrand et al., 2005; Feng et al., 2005) and cavities (Feng et al., 2005). The range of textures and mineral compositions within I-types, however, remains largely undocumented. In this paper we report data on the mineralogy, textures and compositions of a large collection of 88 I-type cosmic spherules collected from Antarctica in order to better characterise these particles and to identify processes that control their textural and compositional evolution during atmospheric entry through which their parent bodies might be constrained. Quantitative criteria to

confidently identify I-type cosmic spherules recovered from sedimentary rocks are also presented.

2. SAMPLES AND METHODS

The spherules reported here were collected from moraine at Larkman Nunatak (86° 46′ S 179° 20′ E) in the eastern Grosvenor Mountains in Antarctica (Fig. 1). Micrometeorites were separated from dry batches of sieved, moraine-derived particles and confirmed as extraterrestrial following protocols described in Genge et al. (2008) and Van Ginneken et al. (2016). Eighty-eight I-type cosmic spherules were identified amongst 1215 micrometeorites on the basis of their high abundances of iron oxides and absence of primary silicates.

Particles were embedded in resin and prepared as polished grain mounts for preliminary backscattered electron imaging (BEI) and analysis by scanning electron microscopy using a Zeiss EVO 15LS SEM at the Imaging and Analysis Centre (IAC) of the National History Museum (NHM) London. Mineral compositions were determined by energy dispersive spectroscopy (EDS) using the Zeiss EVO on polished, carbon-coated samples. Analyses were performed at an accelerating voltage of 15 kV and beam current of 3.0 nA. Cobalt metal and Kakanui augite were used for instrumental calibration. Zeiss matrix corrections were applied against mineral standards. Analyses of iron oxides were corrected by calculating oxygen abundances by stoichiometry, assuming iron present as Fe^{2+}, whilst those of metal were corrected only for observed EDS peaks. Detection limits for EDS analyses are estimated at ~0.3 wt %, whilst analytical uncertainty was estimated at ~5% of values based on two standard deviations.

Major and minor element compositions were determined by wave dispersive spectroscopy (WDS) using a Cameca SX100 at the Natural History Museum in London. Analyses were performed at an accelerating voltage of 20 kV and beam current of 20.0 nA by calibration to a spinel standard for iron oxides, and a metal FeNi standard for metal. Cameca phi-rho-z-based matrix corrections were applied. Detection limits vary by element but average at ~0.05 wt%. All analyses were obtained using spot mode. Matrix overlap suggests a diameter of ~5 μm.

The quality of EDS and WDS analyses was evaluated on the basis of stoichiometry and analytical totals. Matrix overlap was the most significant issue encountered due to the analysis of small phases within a surrounding matrix of a different material, or due to proximity to cavities and grain boundaries. The ideal analytical total for magnetite, where oxygen abundance was calculated assuming only Fe^{2+}, of 93 wt% was used to evaluate the quality of magnetite compositions and analyses with totals within 2% of this value assumed sufficiently accurate. The stoichiometry of wüstite, however, is non-ideal since this mineral can exhibit an oxygen excess of 1.0–4.1 atomic% (0.7–2.9 wt%) as a result of vacancies (from Fe-O phase relations; Darken, 1946). Analytical totals between ~96 and ~100 wt% were taken to indicate wüstite. In cases where crystal size was small EDS analyses provided more accurate stoichiometries owing to less matrix overlap than WDS due to the smaller beam size (~4 μm). Where both EDS and WDS analyses were performed an excellent agreement of ±0.1 wt% Ni was determined for low-Ni wüstite between the techniques. Wüstite with Ni contents at the minimum values of 0.1 wt %, however, could not be reliably detected by EDS.

Phase abundances and crystal sizes were measured using an image analysis tool. Phase abundances were determined by scaled pixel counting by delimiting colour ranges within backscattered electron images by analysis of RGB histograms. Precision of this technique was tested and showed

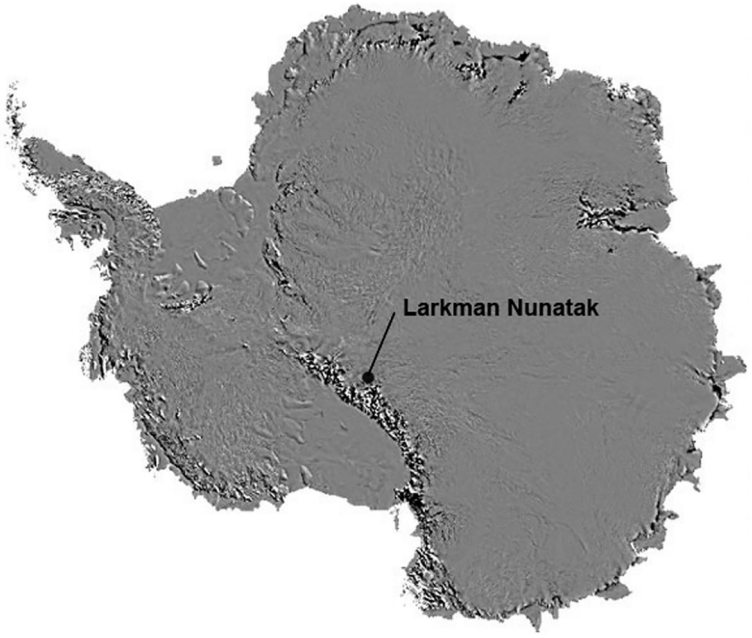

Fig. 1. The location of Larkman Nunatak in Antarctica.

a 2σ error of ~2%. Uncertainty was limited by overlapping color values around fractures and imperfections on the sample surface. Accuracy of phase abundances is subject to plane-of-section effects, in particular for metal beads and cavities which vary in size depending on section. Measurements of phase abundance on metal beads, due to their broadly spherical shapes, are most likely to represent minimum estimates, although the off-centre nature of beads could less frequently result in over-estimate. The curvature of the external surface of spherules was usually visible in BEI of particles cut across small segments allowing an evaluation of the error in area measurements. During polishing most spherules were successfully polished to planes approximately through the median of the particle.

3. RESULTS

The mineralogy and petrology of 88 I-type cosmic spherules from Antarctica are summarised in Table 1. The particles range in diameter from 49 to 231 μm.

3.1. The mineralogy of I-type cosmic spherules

The studied particles have simple mineral assemblages dominated by magnetite (Fe_3O_4) and/or wüstite (FeO) although 44% also contain significant FeNi metal (Figs. 2 and 3). Magnetite and wüstite were both identified in this study on the basis of stoichiometry since neither has polymorphs or amorphous equivalents and their compositions are thus characteristic. Wüstite, however, has oxygen excesses and has the formula $Fe_{1-x}O$ where $x = 0.019$ to 0.079 (Darken, 1946). The structural state of metal was not determined. Representative compositions of the main phases are shown in Table 2 and are within the range of those measured by previous studies of I-types (e.g. Brownlee et al., 1984; Taylor and Brownlee, 1991; Bi et al., 1993). The variations in the relative abundance of magnetite, wüstite and FeNi metal between particles are shown in Fig. 4.

Other phases are present in much smaller abundances in I-type particles. Small (<1 μm) nuggets of platinum-group element (PGE)-rich metal alloy were observed in 10 particles. Although these nuggets were too small for quantitative analysis, EDS spectra suggest that Pt is the most abundant PGE present. Micron-sized Ni-rich Fe alloy nuggets containing detectable Pt were observed in five particles and are distinct from the smaller nuggets that appear to be dominated by Pt.

Hydrous iron oxide replacing FeNi metal is inferred in some particles from its low analytical totals, and can occur either within the cores or rims of metal beads, in particular where these are close to the surface. Analyses of these phases have low totals of 72–84 wt% and are dominated by Fe with minor S (1.0–2.3 wt%), Si (2.0–5.1 wt%), Al (0.5–1.8 wt%), Mg (0.1–0.6 wt%) and Ca (0.1–0.7 wt%). The composition of these phases is similar to ferrihydrite (FeOOH) observed in other micrometeorites (Engrand et al., 1998; Blackhurst et al., 2004; Van Ginneken et al., 2016). Small areas (<2 μm) of Mg-Al-silicates are observed in some particles within interstitial areas. The composition of this phase resembles palagonite including low analytical totals (65–80 wt%) due to water content, significant Si (17.0–22.8 wt%), Al (6.1–16.2 wt%) and variable Mg (0.5–2.4 wt%). Minor amounts (<0.5 wt%) of Ti, Cr and Mn are also present, although their detection may be due to their presence in the surrounding wüstite, and thus an analytical artifact. Compositions of ferrihydrite and palagonite are shown in Table 3. No other phases, such as sulphides or chromite, were identified.

3.2. The textures of I-types

Two general textural groups of I-type spherule were observed in the current study: (1) metal-bearing (MET) spherules (Fig. 2) and (2) metal-free, oxide-dominated (OX) spherules (Fig. 3). Each differs in the texture and mineralogy of its oxide portion, allowing them to be distinguished even in particles where metal is not evident owing to plane of section effects or removal by weathering. Engrand et al. (2005) has previously subdivided I-types into type A, B and C based on magnetite to wüstite ratio in 11 large (>400 μm) I-types, but did not give quantitative or detailed textural criteria or for their distinction. The MET spherules probably correspond to type A spherules, whilst OX correspond to type B and type C. These have also been previously called one oxide and two oxide spherules by Robin et al. (1988). Forty-two MET spherules and 40 OX spherules were observed, of which 11 MET spherules were

Table 1
The abundance of I-types. The abundance of phases and cavities are given in percent cross sectional area of particles.

Textural type		Number	FeNi % Average (range)	Wüstite % Average (range)	Magnetite % Average (range)	Cavity % Average (range)	Diameter (μm) Average (range)
MET	dendritic	18 (20%)	22.9 (91.9–0.0)	75.7 (10–8.8)	0.47 (4.0–0.0)	0.05 (0.7–0.0)	113 (231–62)
MET	homogeneous	24 (27%)	21.7 (49.0–0.0)	78.1 (100–47.0)	0.73 (7.0–0.0)	0.15 (1.8–0.0)	99 (144–49)
OX	magnetite-poor	26 (30%)	0.0	65.8 (97.4–43.9)	34.2 (56.0–34.2)	1.43 (8.9–0.0)	115 (177–65)
OX	magnetite-rich	14 (16%)	0.0	28.0 (45.0–12.3)	72.0 (87.7–55)	2.79 (13.9–0.0)	135 (212–135)
OXMET		6 (7%)	7.3 (18.9–0.0)	67.3 (84.5–55.1)	25.4 (42.8–0.2)	3.0 (5.1–0)	105 (151–72)

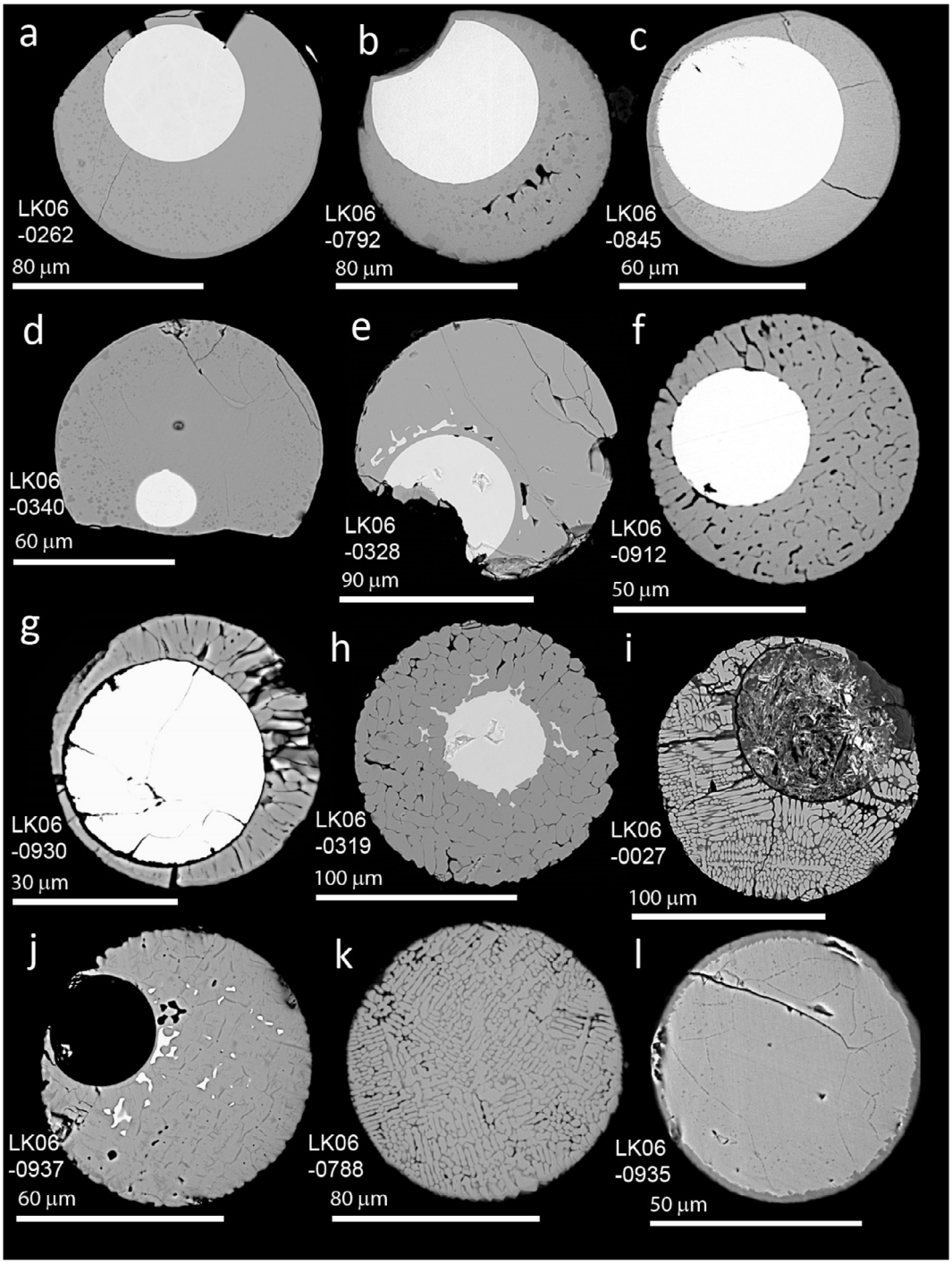

Fig. 2. Backscattered electron images of metal bead-bearing (MET) I-type cosmic spherules. Most particles show relict metal beads, however, metal has been removed by weathering in particles i and j whilst in particles k and l metal beads may not be exposed at the polished surface. Two main textural types are identified: (1) homogeneous wüstite particles (a–e, l) and (2) dendritic wüstite particles (f–k). Metal beads within particles can be smooth (a–d, f, g) or re-entrant with extruded areas of metal (see Fig. 7 for higher resolution images) (e, h, j). Small equant magnetite crystals are present in the wüstite shells of particles and magnetite rims also occur. Magnetite crystals have darker colour in these images than wüstite.

identified on the basis of their oxide textures since metal was not exposed by polishing. A further 6 particles were observed with textures and mineralogies transitional between MET and OX spherules. As these particles contain metal within an oxide mantle containing wustite and magnetite, these are termed OXMET particles. Metal-bearing spherules have broadly the same size range as OX spherules but comprise a larger proportion particles at smaller sizes

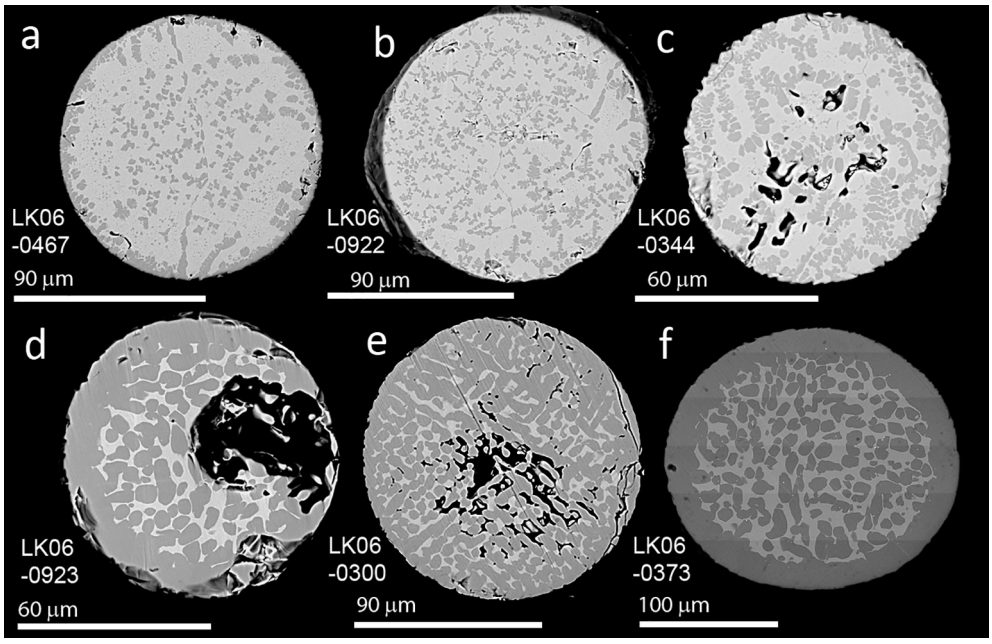

Fig. 3. Backscattered electron images of metal bead free (OX) I-type cosmic spherules. (a–c) Show magnetite-poor spherules containing magnetite dendrites (dark crystals) within wüstite (light areas). (d–f) Show magnetite-rich spherules with coarse magnetite.

with average diameters of 100 μm (MET) compared 119 μm (OX). The cumulative size distribution of MET and OX spherules are shown in Fig. 5 and demonstrate that MET spherules become less abundant relative to OX spherules with increasing size. The size distribution of all particles exhibits a split power law dependence with spherules <120 μm in diameter having an exponent of −1.2 ($R^2 = 0.93$) and larger particles having an exponent of −5.3 ($R^2 = 0.99$).

3.2.1. Metal-bead bearing spherules

Metal-bead bearing (MET) spherules have iron-oxide shells dominated by wüstite and exhibit two distinct textures. Homogeneous spherules have wüstite shells with no observable crystal boundaries and appear to consist of cryptocrystalline wüstite (Fig. 2a–e, and l). In contrast dendritic spherules have obvious wüstite dendrites and usually exhibit cruciform arrangements of parallel sets of bars with cubic arrangement forming a lattice like structure (Fig. 2f, h–k), although some also have radiating morphologies (Fig. 2g). Intersections of bars at angles less than 90° occur owing to a plane of section oblique to crystallographic axes. Average short axis of dendrite bars broadly increases with particle diameter, although with considerable scatter (Fig. 6), although homogeneous wüstite spherules can be any size. The orientation of wüstite dendrites in most spherules is random relative to the metal bead, however, in particles where a sizeable metal bead (>40% of particle diameter) approaches the surface of the particle dendrites often radiate away from the bead (Fig. 2g). Cavities are often present between dendrites, although in some particles these interstitial regions are filled with palagonite (Fig. 7a).

Homogeneous and dendritic MET I-types both contain small amounts of magnetite as discrete grains and thin (<10 μm) external rims. In homogeneous MET spherules discrete crystals of magnetite tend to occur as small (<5 μm) equant grains that usually show an increase in abundance towards the exterior of the particle, which is often greatest in the direction that the metal bead is offset from the centre (Fig. 7c). Trails of equant magnetite crystals are observed in some homogeneous particles (Fig. 7c). In dendritic MET particles magnetite occurs as irregular grains likewise concentrated towards the external margin of the particle (Fig. 7d). External magnetite rims are present on all metal bearing particles, although they may be very thin (<1 μm). Most have facetted internal margins. The width of magnetite rims is often largest, by a factor up to 10, on the side of the particle nearest offset metal beads (Fig. 7f).

Metal beads range widely in proportions from a maximum of 91% of particle cross-sectional area to 5.4% with an average of 33.6% (Fig. 4). Most metal beads (77%) within I-types have smooth circular outlines, however, those located close to the outer surface sometimes exhibit non-circular shapes with short axes oriented towards the nearby particle surface (Fig. 2c and d). In no particle, however, was the metal bead exposed at the surface; instead a thin outer veneer of iron-oxide was always observed covering the metal bead (Fig. 2b and 7e, f). In some particles a thicker rim, usually of magnetite, was observed that forms a lobate indent extending into the metal bead (Fig. 2e and 7g). Some particles with near-surface metal beads have non-spherical particle shapes exhibiting a decrease in curvature (Fig. 2a and c) or an indented pit (Fig. 2b, d, and e) overlying the bead. In one particle small inclusions of iron oxide were observed within metal at the margin of the particle (Fig. 7e).

Table 2
Showing representative compositions of metal, wüstite (wus) and magnetite (mag) in wt%. Oxygen abundance is calculated by stoichiometry for oxides assuming iron is divalent. Ideal total for magnetite is 94% whilst wüstite varies from 96 to 100%. Analyses presented to two decimal places were determined by WDS whilst all others were determined by EDS.

Particle	LK06-0248	LK06-0258	LK06-0341	LK06-0344	LK06-0595	LK06-0623	LK06-0815	LK06-0921	LK06-0922	LK06-0923	LK06-0924	LK06-0927	LK06-0932	LK06-0936	LK06-1040	LK06-1048	LK06-1053	LK06-1139	LK06-0013	LK06-0081
Phase	mag	mag	mag	mag	mag	mag	mag	mag	mag	mag	mag	mag	mag	mag	mag	mag	mag	mag	metal	metal
Fe	71.64	68.97	66.91	65.16	62.7	66.5	71.2	67.52	68.06	71.27	65.46	68.5	67.21	68.5	69.2	71.2	67.7	69.80	40.2	59.47
Ni	0.32	3.54	6.38	6.57	9.1	6.9	1.5	5.31	4.50	1.02	5.73	4.3	5.82	4.1	2.9	1.0	4.3	3.40	59.2	39.08
Co	–	–	–	–	–	–	–	–	–	–	–	–	–	–	–	–	–	–	3.3	1.52
Cr	0.22	–	–	–	–	–	–	–	–	0.09	0.12	–	0.06	–	0.5	–	–	–	–	–
O	20.72	21.01	20.88	20.48	20.7	20.9	20.8	20.76	20.79	20.72	21.10	20.8	20.86	20.8	20.8	20.7	20.6	20.98	0.0	0.0
Totals	92.90	93.54	94.17	92.23	92.5	94.3	93.5	93.59	93.35	93.10	92.41	93.6	93.95	93.4	93.4	92.9	92.6	94.18	102.7	100.09

Particle	LK06-0262	LK06-0278	LK06-0278	LK06-0319	LK06-0328	LK06-0340	LK06-0853	LK06-0854	LK06-0885	LK06-0904	LK06-0912	LK06-0925	LK06-0928	LK06-0930	LK06-0931	LK06-0937	LK06-0027	LK06-0081	LK06-0242	LK06-0248
Phase	metal	metal	metal[a]	metal	metal	metal	metal	metal	metal	metal	metal	metal	metal	metal	metal	metal	wus	wus	wus	wus
Fe	48.62	52.18	48.26	58.68	65.35	28.08	6.5	37.2	74.9	77.6	76.0	62.90	75.4	88.75	74.32	27.10	73.68	74.83	66.56	74.56
Ni	48.51	41.58	49.78	38.82	33.63	70.86	93.7	59.8	21.1	20.9	22.0	35.07	23.3	10.87	24.80	70.45	0.10	0.27	8.59	0.59
Co	2.75	1.30	1.93	2.78	1.43	2.00	–	4.0	2.6	–	–	1.46	–	0.50	1.01	1.08	–	–	–	–
Cr	–	–	–	–	–	–	–	–	–	–	–	–	–	–	–	0.45	0.18	–	–	0.04
O	0.0	0.0	0.0	0.0	0.0	0.0	0.0	0.0	0.0	0.0	0.0	0.0	0.0	0.0	0.0	0.0	22.80	22.21	21.39	21.68
Totals	99.89	95.07	99.97	100.28	100.42	100.94	100.2	101.0	98.6	98.5	98.0	99.45	98.7	100.13	100.15	99.08	96.76	97.32	96.54	96.87

Particle	LK06-0248	LK06-0254	LK06-0258	LK06-0262	LK06-0278	LK06-0308	LK06-0319	LK06-0328	LK06-0340	LK06-0341	LK06-0344	LK06-0919	LK06-0920	LK06-0922	LK06-0924	LK06-0925	LK06-0926	LK06-0930	LK06-0931	LK06-0932
Phase	wus	wus	wus	wus	wus	wus	wus	wus	wus	wus	wus	wus	wus	wus	wus	wus	wus	wus	wus	wus
Fe	74.56	69.60	70.94	75.20	75.20	75.08	75.44	76.19	74.74	65.74	63.52	70.11	74.52	68.86	63.53	76.43	69.19	73.69	74.39	65.89
Ni	0.59	5.41	4.16	0.35	0.28	0.64	0.21	0.14	0.79	8.62	11.31	1.15	0.65	6.82	10.82	0.17	6.51	0.35	0.16	6.76
Co	–	–	–	–	–	–	–	–	–	–	–	–	–	–	–	–	–	–	–	–
Cr	0.04	–	0.04	–	–	–	–	0.38	0.17	–	–	0.57	–	–	0.33	0.15	0.10	0.24	0.55	0.12
O	21.68	21.56	21.57	21.65	22.05	21.68	21.89	22.04	21.73	21.18	21.34	22.26	22.10	21.62	21.84	22.01	21.62	21.93	21.70	22.10
Totals	96.87	96.57	96.71	97.20	97.53	97.41	97.56	98.75	97.43	95.55	96.18	94.09	97.28	97.30	96.52	98.76	97.42	96.21	96.80	94.87

[a] Metal extruded into oxide mantle. All other analyses are of metal beads.

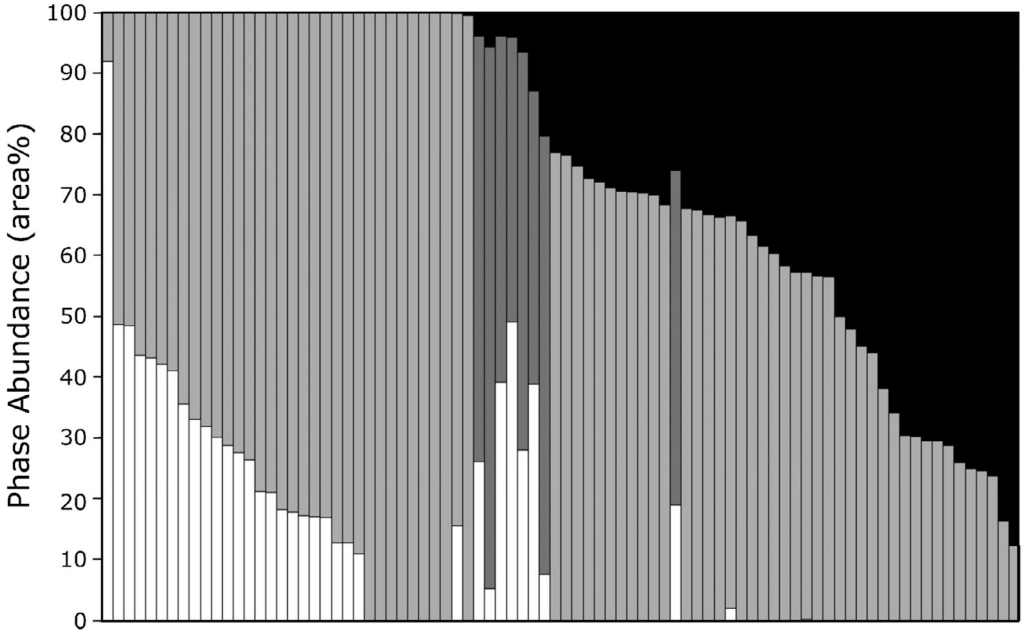

Fig. 4. The cumulate size distribution of I-type cosmic spherules. Grey markers show OX spherules which dominate at large sizes.

Table 3
Compositions of alteration phases in wt%. Matrix overlap with surrounding wüstite is likely for palagonite. Oxygen is calculated by stoichiometry assuming divalent iron. A dash indicates data is below detection limits.

Particle	Phase	Mg	Fe	Ni	Al	Si	Ca	K	S	Cl	Ti	Cr	Mn	O	Totals
LK06-0027	ferrihydrite[a]	0.51	51.41	1.83	1.20	3.85	0.62	–	1.16	–	–	–	–	23.02	83.6
LK06-0929	ferrihydrite[a]	0.3	41.0	1.3	1.7	4.3	0.5	0.2	1.5	0.9	–	–	–	21.2	72.9
LK06-0937[b]	palagonite	1.11	7.42	0.04	15.99	17.54	0.19	–	–	–	0.23	0.23	0.04	37.43	80.23
LK06-0919	palagonite	0.53	1.94	–	6.75	22.79	0.14	–	–	–	0.10	–	–	33.01	65.29

[a] Material is likely to be an assemblage of phases dominated by ferrihydrite or goethite.
[b] EDS analysis.

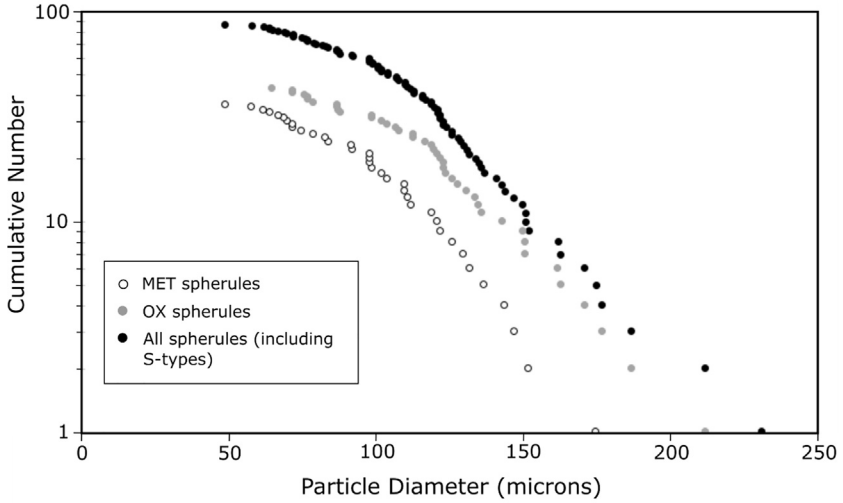

Fig. 5. Abundance of metal (white), wüstite (grey) and magnetite (black) within individual particles. Particles are arranged horizontally by increasing magnetite to wüstite ratio. OXMET spherules have wüstite shown as dark grey.

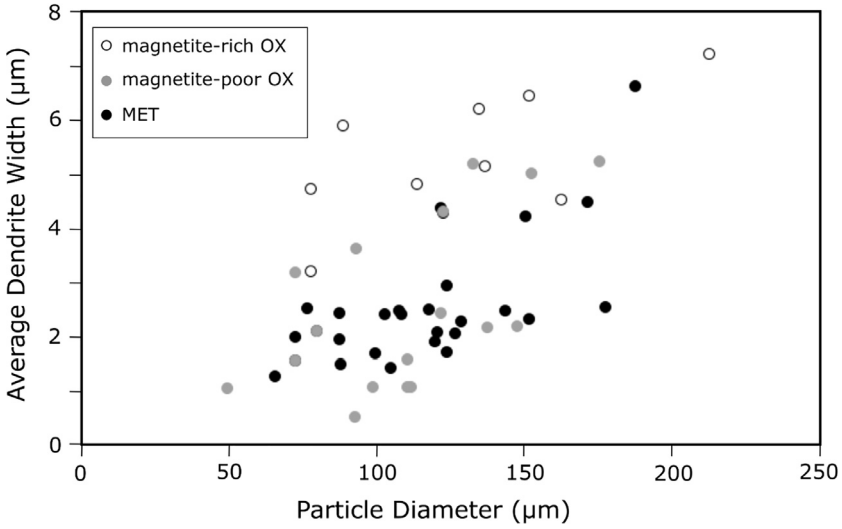

Fig. 6. Crystal sizes of wüstite and magnetite within I-type cosmic spherules.

In 23% of MET particles metal beads have re-entrant rather than smooth surfaces with protrusions of metal penetrating outwards along grain boundaries of wüstite dendrites (Fig. 2h and j). Metal protrusions were observed as continuous veins of metal and as isolated intergranular metal at wüstite triple junctions (Fig. 7h). In one particle with metal protrusions (LK06-0278) a smooth lenticular cavity was observed on one side of the metal bead (Fig. 7i). Smooth and re-entrant metal beads are not compositionally distinct from each other, however, metal interstitial to wüstite dendrites often has higher Ni and Co concentrations than the coexisting metal bead.

Some MET spherules exhibit spherical, fine-grained polycrystalline masses of ferrihydrite with fibrous or platy individual sub-micron crystals, sometimes with relict FeNi metal (Fig. 2i) indicating that these are weathering products. Ferrihydrite is identified on the basis of composition, low analytical totals and habit. Partial alteration can occur either on the exterior of the metal bead or within the core (Fig. 7h). In several particles off-centre spherical cavities occur and are similar in size and location to metal beads (Fig. 2j). Rims of ferrihydrite also extend over the external surface of 3 MET particles (Fig. 7j).

In 26% of MET spherules no metal bead was observed in the plane of section (Fig. 2k). These are interpreted as MET spherules owing to their low magnetite contents (<5 vol%) and wüstite textures (dendritic or homogeneous). Furthermore, five particles have sub-spherical voids interpreted as forming by weathering and removal of metal or ferrihydrite rims after metal.

3.2.2. Metal bead-free spherules

Metal bead-free, oxide-dominated (OX) spherules consist of mixtures of magnetite and wüstite. Two textural varieties were observed: (i) magnetite-poor spherules (<50 vol% magnetite) which exhibit fine-grained (widths < 5% of particle diameter), re-entrant dendritic magnetite crystals within a groundmass of homogeneous wüstite (Fig. 3a–c), and (2) magnetite-rich spherules (50–88 vol% magnetite) which exhibit smooth, coarser magnetite crystals varying from elongate barred dendrites to equant grains within homogeneous wüstite (Fig. 3d–f). Fourteen magnetite-rich spherules were observed out of the 40 OX spherules. A broad positive correlation exists between the short axis dimensions of magnetite crystals with particle diameter (Fig. 6).

In magnetite-poor OX spherules dendritic crystals of magnetite consist of a series of lobate parallel protrusions arranged perpendicular to the length the crystal (Fig. 9a). Some dendrites, in particular in those spherules with higher abundances of magnetite, however, occur as elongate crystals without perpendicular lobate protrusions (Fig. 9b and c). A characteristic feature of the dendrites is the presence of some radiating clusters of crystals comprising three individuals arranged at approximately 120° to each other (Fig. 9a), in addition to the 90° intersections typical of cruciform dendrites (Fig. 9c). Often dendrites are more abundant close to the external surface of the spherule (Fig. 3a). In one particle (LK06-0924) elongate bifurcating cavities are present close to the centre of many magnetite crystals (Fig. 9c and e). Magnetite veins <1 μm in width were observed within some OX particles (Fig. 9g).

Although lacking FeNi metal beads, some OX spherules contain micron (<2 μm) to sub-micron Ni-rich metal grains. In magnetite-rich and poor particles Ni-rich metal (>90 wt % Ni) can also occur in abundance within symplectic rims surrounding magnetite crystals (Fig. 9e and f). Isolated sub-micron Ni-rich metal and PGE nuggets were also observed as inclusions mainly within magnetite crystals within magnetite-rich spherules (Fig. 9h) and as trails within veins of magnetite (Fig. 9g).

Magnetite rims around the exterior of particles were observed on most OX spherules and range from <2 to 12.5 μm in width (Fig. 3). Rim thickness was determined as an average of ten measurements within each particle. Magnetite rims sometimes include small facetted inclusions

of wüstite and tend to be thickest on the largest spherules (Fig. 10).

A proportion of OX spherules contain cavities that comprise up to 8.9% of the cross-sectional area (Fig. 3c–e). The cavities are usually present as rounded, irregular voids; however, in several particles they occur as an interconnected network that trace intergranular areas between either magnetite or wüstite crystals. Cavities are most common within the centre of particles. No correlation is observed between particle size or magnetite abundance with the abundance of cavities.

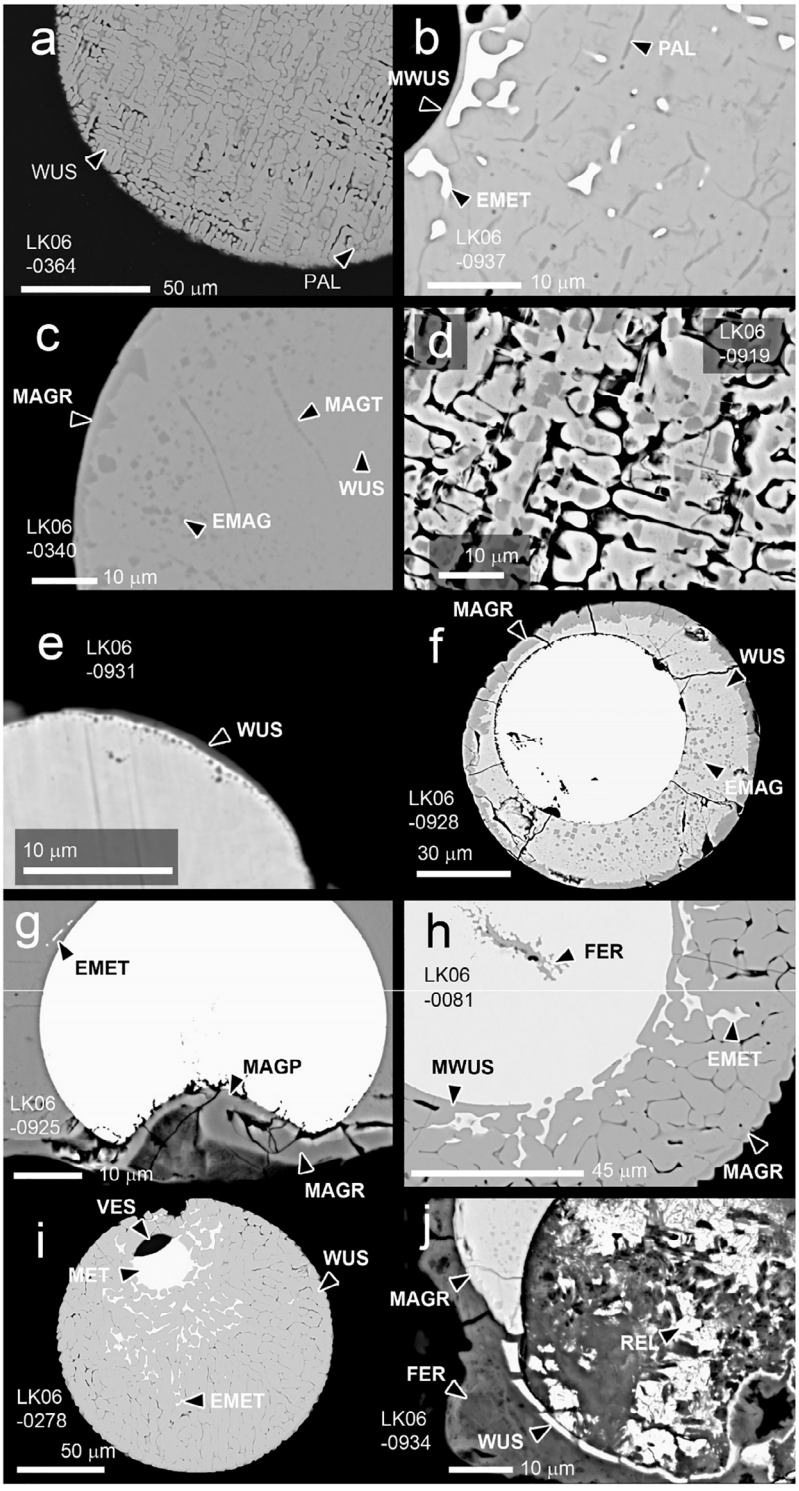

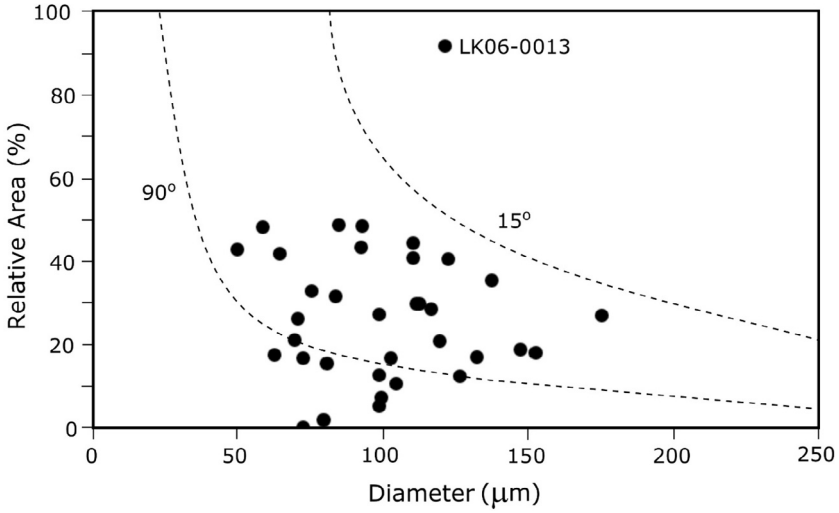

Fig. 8. The relative area of metal beads compared with particle diameter. The dashed lines show the predictions of the entry heating model of Genge (2016) for an entry velocity of 12 km s^{-1}. The relative area is likely to be a minimum estimate in most cases due to plane of section effects. Particle LK06-0013 is anomalously Ni-rich compared to its size and likely to have a taenite precursor.

3.2.3. OXMET I-types

Six I-type spherules were observed that share mineralogical and textural features with both MET and OX spherules; these are referred to as OXMET I-types (Fig. 11). Particle LK06-0678 contains a metal bead with a smooth outline except on one side where an indent of wüstite occurs (Fig. 11a). The oxide mantle contains magnetite dendrites within wüstite, with magnetite abundances typical of OX spherules. A half-moon shaped cavity is also present. Magnetite dendrites are most abundant around the margin of the spherule and adjacent to the cavity.

Three similar particles exhibit (~5 μm) sub-spherical metal beads located on one side of the spherules and surrounded by a mantle of wüstite containing little magnetite (Fig. 11b). The remainder of the particles contain magnetite dendrites and rounded elongate cavities similar to OX particles. All OXMET particles exhibit metal beads with higher Ni contents (up to 94.9 wt% Ni) than those in MET particles (up to 70.5 wt% Ni). The Ni content of wüstite within these spherules is also higher than in most OX spherules at 9.0–22.5 wt% compared with 0.6–12.7 wt%.

Two magnetite-poor OXMET spherules exhibit spherical smooth cavities, with diameters and positions similar to those of metal beads, with mantles of wüstite (Fig. 11c). Both particles also contain irregular smooth cavities. These are interpreted as OXMET spherules in which metal has been removed by weathering.

3.3. External morphology

Most I-types have a high degree of sphericity, however, a small proportion have a crater-like indents with decreased curvature on one side and thus diverge from perfect spheres (Fig. 12b). In cross-section spherules with surface indents have metal beads close to the surface.

In both MET and OX spherules dendritic crystal forms appear on the surface, often as cruciform dendrites with two sets of cross-cutting parallel bars (Fig. 12a and h), however, some also exhibit a pattern of cellular-like crystal forms (resembling the intersection of equant cells) in some areas (Fig. 12b and f). Within dendritic OX spherules the surface crystals do not, however, match the positions of interior magnetite dendrites and instead appear to represent intergranular wüstite crystals (Fig. 12h). Magnetite dendrites within these particles align with the grain boundaries of wüstite crystals observed on the surface. Within

Fig. 7. Showing textural and mineralogical features of MET spherules. (a) Palagonite (PAL) partially filling interstitial areas between wüstite (WUS) dendrites. (b) Palagonite (PAL) filling interstitial areas between wüstite dendrites in a particle with wüstite mantling (MWUS) a smooth spherical cavity. It also contains extruded metal (EMET). (c) Equant magnetite crystals (EMAG) within homogeneous wüstite (WUS). Equant crystals increase in size towards the exterior of the spherule. Trails of magnetite crystals (MAGT) and a magnetite rim (MAGR) also occur. (d) Irregular magnetite crystals within lighter wüstite dendrites. (e) Wüstite veneer (WUS) on a metal bead at the surface of a particle. Small inclusions of iron oxide also occur within the metal. (f) A non-spherical particle with a magnetite rim (MAGR) best developed in the offset direction of the metal bead. A depletion in equant magnetite (EMAG) occurs close to the rim. (g) A smooth metal bead with some extruded metal (EMET) in the wüstite mantle. The particle exhibits a magnetite rim (MAGR) which penetrates the metal bead (MAGP), (h) A re-entrant metal bead with metal extruded (EMET) between wüstite dendrites. Mantling wüstite (MWUS) surrounds the metal bead. A small area of ferrihydrite is present in the core of the metal bead. The particle has a magnetite rim (MAGR) (i) A particle with a re-entrant metal bead (MET) surrounded by extruded metal (EMET). A vesicle (VES) occurs within the metal bead. (j) Ferrihydrite replacing metal and forming an external rim (FER). A thin, broken veneer of wüstite is preserved (WUS) and relict metal is present (REL). The particle has a thin magnetite rim (MAGR).

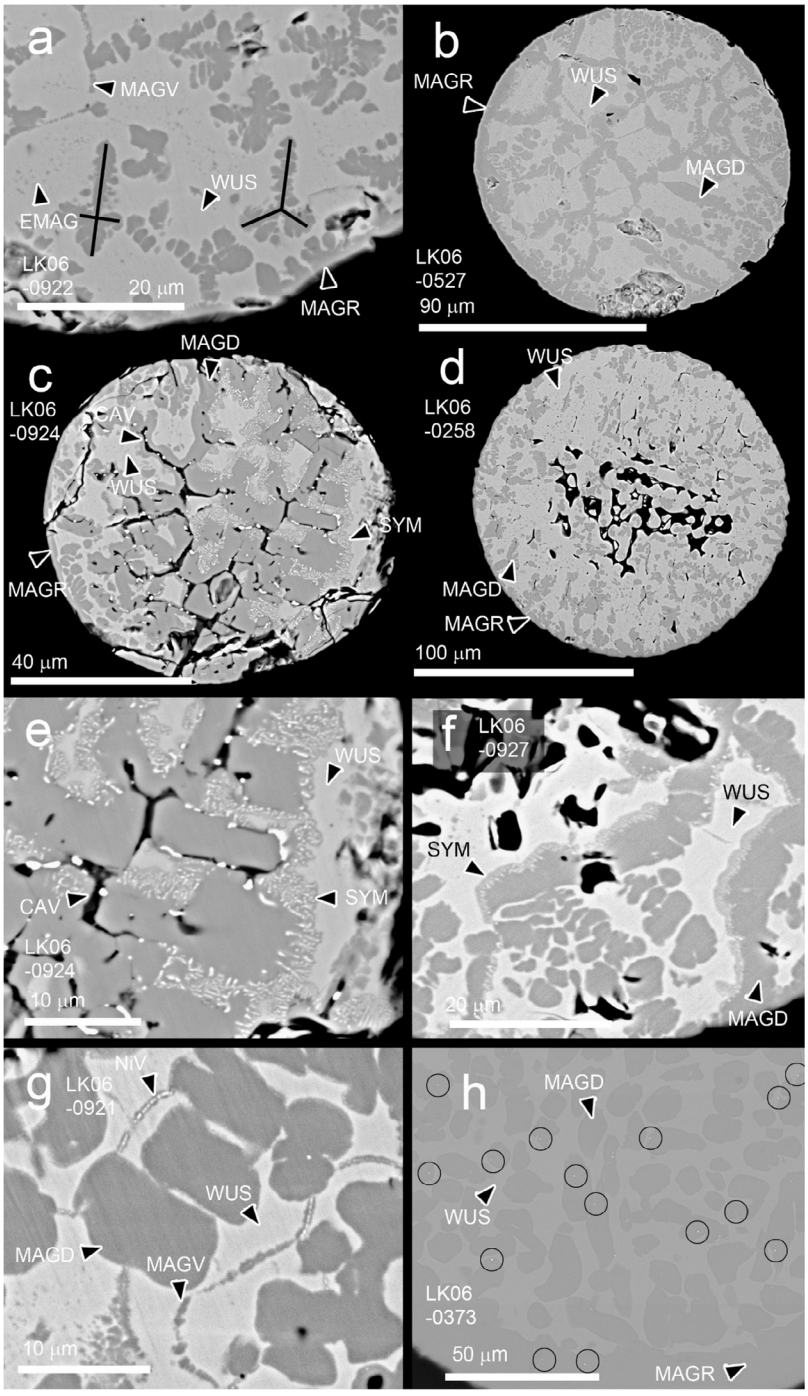

Fig. 9. Mineralogical and textural features of OX spherules. (a) Magnetite dendrites consisting of parallel lobes within interstitial wüstite. Some dendrite have 120° intersections. Sub-micron equant magnetite crystals (EMAG) appear in wüstite (WUS) between magnetite dendrites. Veins of magnetite (MAGV) and a magnetite rim (MAGR) are also present. The elongation directions dendrites are shown by black lines. (b) Lobate dendrites of magnetite (MAGD) forming a network-like structure of crystals with clear 120° intersections within wüstite (WUS). A magnetite rim (MAGR) is also present. (c) Dendrites of magnetite (MAGD) centred on linear, branching cavities (CAV) within wüstite (WUS). This particle also exhibits symplectites (SYM) and a magnetite rim (MAGR). (d) Cavities between wüstite dendrites (WUS) in a magnetite-poor spherule. The location and shape of cavities is not controlled by magnetite dendrites (MAGD). (e) Symplectites of magnetite and Ni-rich metal (SYM) in at the boundary between magnetite dendrites and surrounding wüstite (WUS). Larger grains of Ni-rich metal appear adjacent to linear cavities (CAV). (f) Symplectites of magnetite and Ni-rich metal (SYM) at the margins of magnetite dendrites within wüstite (WUS), (g) Veins containing trails of Ni-rich, Pt-bearing metal nuggets (NiV) within a particle containing magnetite dendrites (MAGD) within wüstite (WUS) and magnetite veins (MAGV). (h) Locations of abundant Pt-group element nuggets within a magnetite-rich particle containing magnetite dendrites (MAGD) within wüstite (WUS) and having a magnetite rim (MAGR).

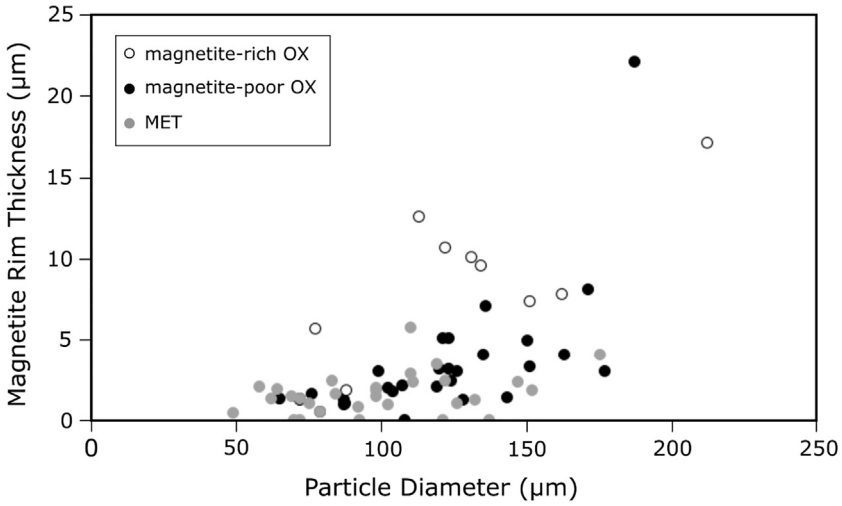

Fig. 10. Magnetite rim thickness on I-type spherules.

magnetite-rich OX spherules having barred magnetite, surface crystals correlate with those of internal magnetite. Particles with thick magnetite rims can also exhibit surface dendrites, typified by their branching structure, albeit somewhat less well defined (Fig. 12g). Some magnetite-poor spherules exhibit poorly defined or no dendritic surface features having instead multiple domains exhibiting parallel facets (Fig. 12e). Metal bead-free spherules sometimes also exhibit surface cavities, sometimes with a cylindrical shape (Fig. 12e). Magnetite-rich OX particles that have equant crystals commonly exhibit similar equidimensional crystal forms on their surface often with multiple parallel steps on crystal faces (Fig. 12c and i). Only a single homogeneous MET spherule was imaged and it exhibits indistinct fine-grained dendrites on its exterior.

3.4. Phase chemistry

The compositions of magnetite, wüstite and metal vary significantly between I-type particles. Iron-nickel metal within metal beads varies in Ni content from 10.9–95 wt% and includes detectable Co with Ni/Co mass ratios of 14.0–35.4, although one particle (LK06-0013) has a ratio inferred from Co detection limit of >100. A broad negative correlation exists between Ni content and the fractional cross sectional area of the metal bead. One outlier, a single large metal bead in particle LK06-0013 has a high Ni content of 59.1 wt% (Fig. 13). Dispersed metal, extruded from metal beads, has up to 10 wt% higher Ni contents than in the parental metal beads, but the same Ni/Co ratios within error. In particle LK06-0937 (Fig. 2j), extruded metal also contains 0.45 wt% Cr. No other elements are within WDS detection limits in metal beads and their compositions are homogeneous to within error.

Metal within symplectic rims on magnetite within OX spherules has high Ni contents at >30–40 wt% but has no detectable Co by EDS, although significant matrix overlap with surrounding oxides occurs. Nickel-rich, sub-micron beads could not be quantitatively measured due to beam overlap with surrounding phases. High Ni contents of >80 wt% Ni in analyses of areas with these beads, compared with the low Ni contents in areas without them, confirms their high Ni contents.

The Ni contents of wüstite vary widely from 0.1 to 22.5 wt%. Wüstite coexisting with metal in MET spherules has low Ni contents of 0.1–1.5 wt% with an average of 0.35 wt%. Nickel contents in wüstite within these particles exhibit a broad positive correlation with the Ni abundance within the coexisting metal (Fig. 14). Compositional variability in wüstite was observed in several MET particles with Ni contents up to 1 wt% Ni higher in thin veneers between a metal bead and the surface (HWUS, Fig. 14). Wüstite in many MET particles with dendrites experience some matrix overlap with Mg-Al-silicates (interpreted as palagonite) within intergranular areas and as a consequence Mg, Al, Ca and Mn are present in many analyses and thus were rejected as poor analyses of the oxide phase. Within OX spherules wüstite has mostly higher Ni contents of 0.6–12.7 wt% with an average of 6.07 wt% than in MET spherules. Chromium contents of up to 1.57 wt% are observed within wüstite in 22 I-types, including MET and OX spherules. The highest Cr content in wüstite was observed in particle LK06-0937 (Fig. 2j) which also contains detectable Cr in extruded metal.

Magnetite compositions in OX spherules vary from 0.31 to 7.53 wt% Ni with an average of 4.35 wt%. Magnetite always has lower Ni contents than coexisting wüstite, and a positive correlation exists between wüstite and magnetite Ni contents (Fig. 15). Magnetite rims have compositions similar to those of dendrites but can have Ni contents that differ by ±1 wt%. Chromium contents are generally below detection limits, although five magnetites had detectable Cr abundances of up to 0.5 wt%. In two particles coexisting wüstite also contained Cr with values approximately double that of magnetite, although a lower value was also observed in one particle.

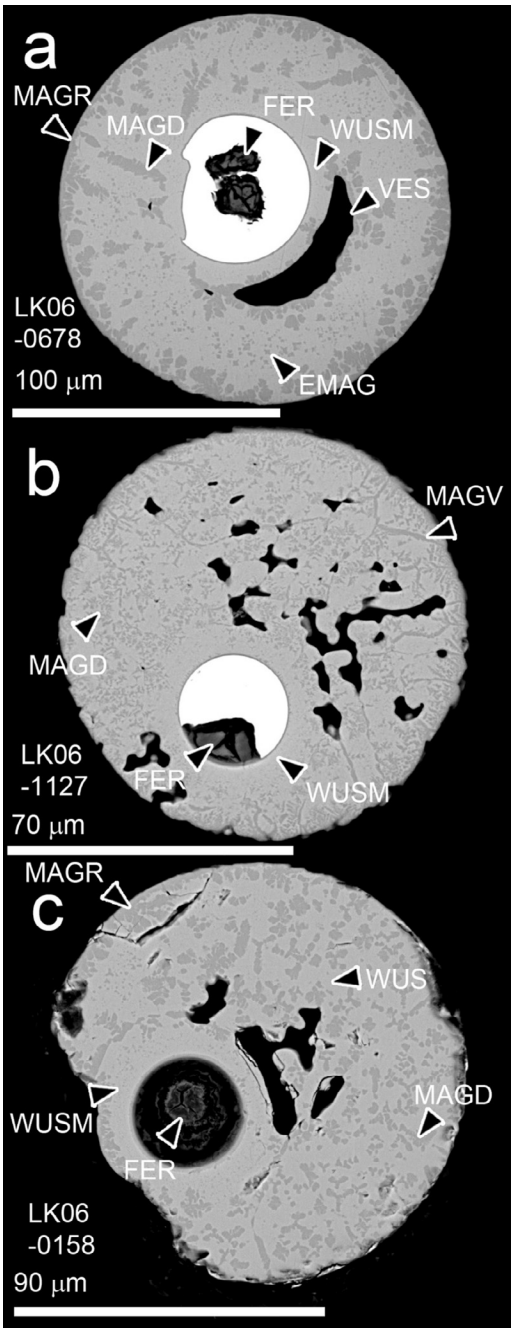

Fig. 11. Showing transitional I-type particles exhibiting features of both MET and OX spherules. (a) Particle "Mikey" has a central, non-spherical metal bead, which is partially altered to ferrihydrite (FER), surrounded by a shell of wüstite containing dendritic magnetite. The wüstite mantle (WUSM) contains a lenticular cavity (VES) decorated by magnetite dendrites (MAGD) and a magnetite rim (MAGR). (b) A particle containing a small metal bead, partially altered to ferrihydrite (FER), surrounded by a wüstite and magnetite mantle containing abundant rounded irregular cavities. The metal bead is mantled by magnetite-poor wüstite (WUSM) and veins of magnetite also occur (MGV). Magnetite dendrites (MAGD) are unusually small in this particle. (c) A particle containing a spherical void after metal, containing some ferrihydrite (FER), surrounded by a mantle of wüstite (WUSM). The remaining shell contains magnetite dendrites (MAGD) within wüstite (WUS) and contains rounded, irregular cavities.

4. DISCUSSION

4.1. Formation by melting and oxidation of FeNi metal grains

The morphology of I-types spherules is consistent with the consensus view that these particles form by the melting and oxidation of extraterrestrial metal dust particles during atmospheric entry heating (Brownlee, 1985; Yiou et al., 1985; Bonte et al., 1987; Herzog et al., 1999; Engrand et al., 2005; Feng et al., 2005; Genge, 2016). The presence of metal beads and the wide variation in metal content from 0.2 to 91 area % supports the melting of solid grains of FeNi during entry heating since it suggests, along with the spherical shape of particles, that these particles form as liquid metal droplets that were progressively oxidised. The rarity of unmelted metal grains is thought to be the result of their intense atmospheric entry heating owing to their high densities. Numerical models show that metal particles >40 μm in diameter even at low entry velocities of 12 km s^{-1} with survival of metal at larger sizes restricted to rare low angle, grazing incidence encounters (Genge, 2016).

The formation of I-types by separation of immiscible metal beads from S-type micrometeorites or larger meteoroids, however, could generate similar textures. Observations that the size distribution of I-type spherules is not significantly smaller than S-types (Bonte et al., 1987) and that S-types contain smaller metal droplets (Genge and Grady, 1998), suggests that immiscible separation from other micrometeorites is not a significant source of I-types (Herzog et al., 1999). Formation by separation as ablation spherules from larger meteoroids (Blanchard et al., 1980; Brownlee and Bates, 1983) can also be discounted as a major source since the flux of cosmic spherules to the surface is significantly larger than that of meteorites (1600 t/a compared with 10 t/yr – calculated assuming 90% mass loss for meteorites during atmospheric entry; Love and Brownlee, 1993; Bland et al., 1996; Taylor et al., 2000). Perhaps most conclusive, however, is the observation of appreciable ^{10}Be within large I-types, since the highly lithophile nature of Be would ensure very low abundance in I-types if they formed by immiscible separation from silicates (Yiou et al., 1985). Large I-types were, therefore, exposed to radiation in interplanetary space as dust-sized metallic objects.

Evidence for the oxidation of metal during entry heating is provided by the iron oxide-dominated shells of I-types and their oxygen isotope compositions, which are consistent with those expected from mass-dependent fractionation of terrestrial atmospheric oxygen (Herzog et al., 1999; Engrand et al., 2005). The range of metal abundances agrees with simulations of the atmospheric entry of I-types, which suggest that oxidation increases with entry angle and particle size due to penetration to lower altitudes and heating under higher partial pressures of oxygen (Genge, 2016). The abundance of metal within spherules compared to particle diameter thus is dependent on the entry parameters (Fig. 8), and on the initial size (Genge, 2016). The observation that MET spherules have a smaller average size than OX spherules (Fig. 5) is consistent with the strong influence

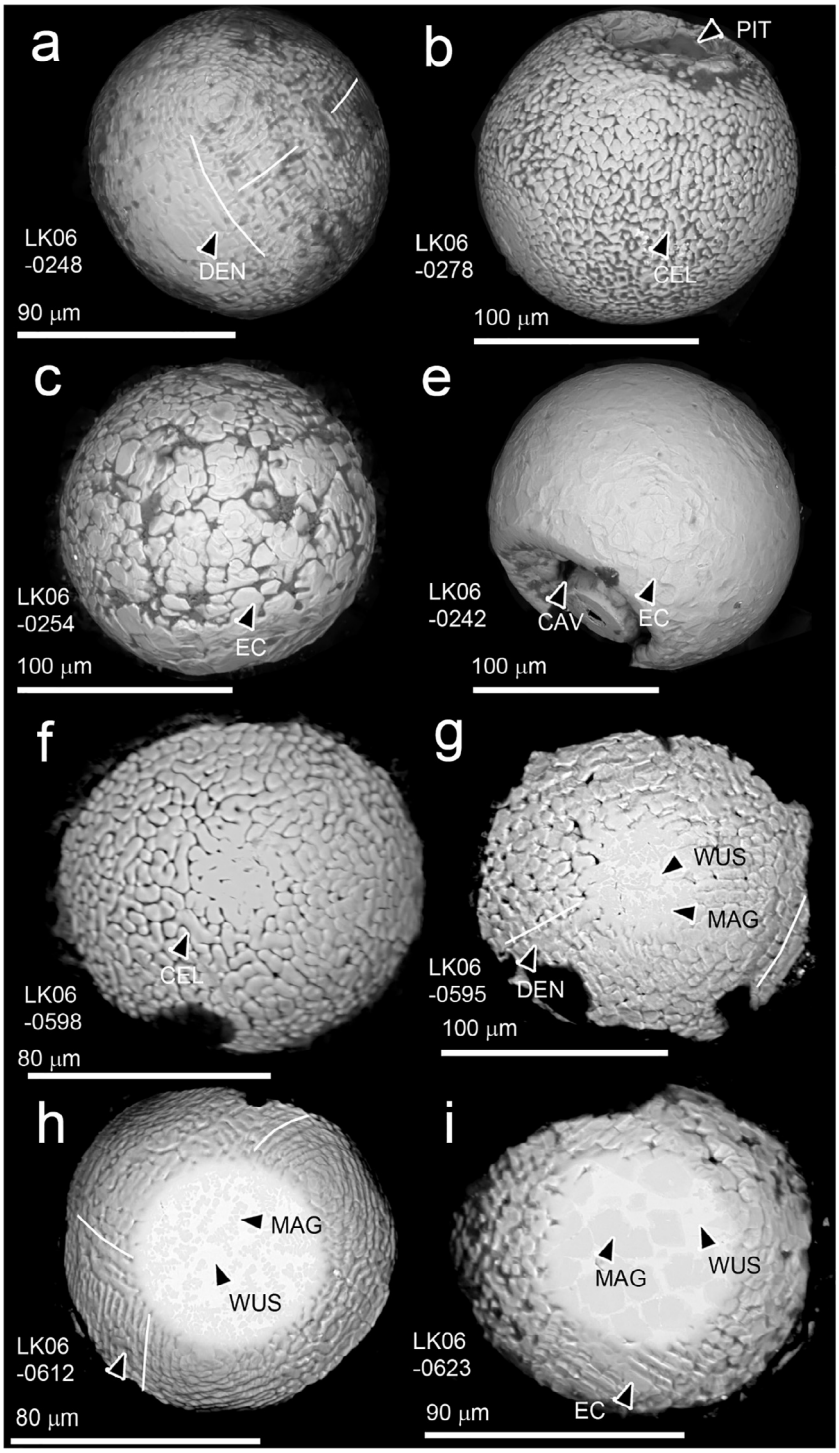

Fig. 12. The external morphology of I-type spherules. Most MET and OX spherules exhibit dendritic crystal morphologies (labelled DEN with white lines showing main elongation directions) on their surfaces (a, b, f, g and h) which relate to wüstite crystals. MET spherules generally have the best defined dendrites (b, f) whilst OX spherules show some modification by magnetite dendrites (a, g, h) resulting in less well defined crystal shapes. Magnetite-rich spherules with equant crystal morphologies often show equidimensional crystal forms (EC) on their surface (c, i) which have step-like planar features. MET spherules sometimes exhibit pits on their outer surface due to the deformation of spherules as the bead approaches the surface (PIT) (b). OX spherules sometimes exhibit cavities on their surfaces which are sometimes cylindrical (CAV) (e). The upper part of particles f, g, h and i have been polished to reveal the interior texture. Magnetite (MAG) and wüstite (WUS) can be seen in the interior of particles g, h and i.

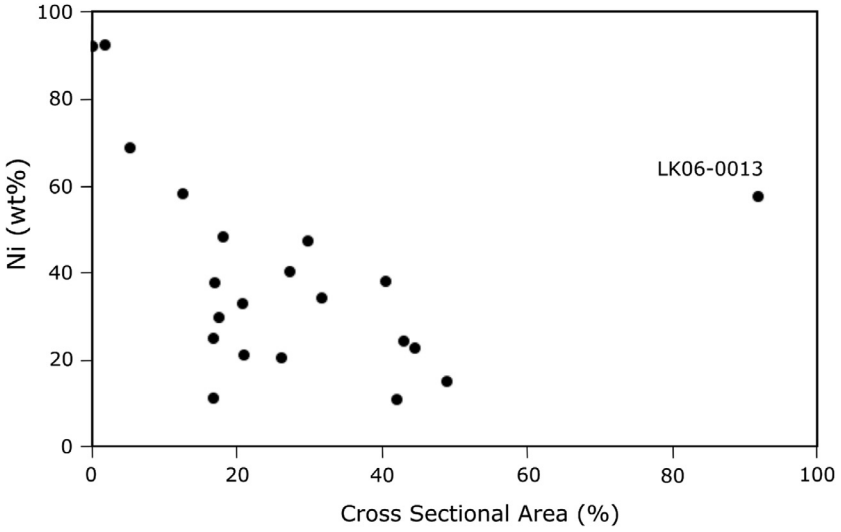

Fig. 13. The Ni-content of metal beads compared with relative cross sectional area. Due to plane of section effects the cross sectional area is likely to be a minimum. Particle LK06-0013 has high Ni for its size and may have a taenite precursor.

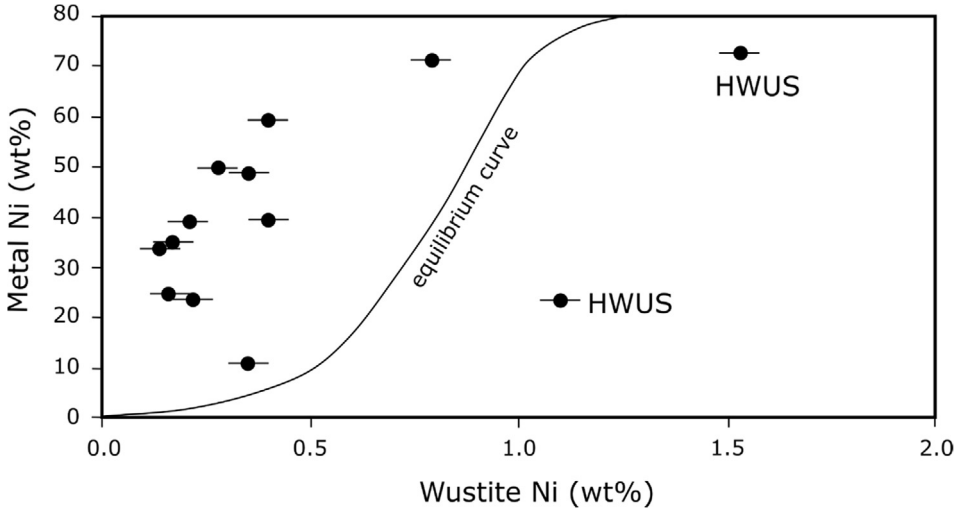

Fig. 14. The Ni contents of coexisting wüstite and metal within MET spherules compared with the equilibrium partitioning curve derived from Fe-Ni-O phase relations (Raghavan, 2010). Higher Ni wüstite (HWUS) occurs located close to the leading edge of the particle adjacent to metal beads.

of particle size on the altitude of peak heating, and thus the partial pressure of oxygen under which heating occurs. Previous studies have also noted that most metal-bead-bearing deep sea I-types have diameters <150 μm (Brownlee et al., 1984), with only rare examples of larger size that could be explained by low entry angles that allow survival of metal (Genge, 2016). Isotopic studies of I-type spherules also reveal an increase in heating and evaporation with magnetite content (Engrand et al., 2005) consistent with the peak temperatures predicted by Genge (2016) which increase with particle size and entry angle.

The smooth spherical nature of the majority of metal beads and the dendritic habits of iron oxide crystals (Fig. 2) indicates that oxidation occurs principally in the liquid state, with an immiscible oxide liquid growing from a metal liquid, followed by very rapid cooling. Oxidation experiments conducted on solid metal, in contrast, demonstrate that irregular surfaces develop at the metal-oxide interface (e.g. Young, 2008; Krzyzanowski et al., 2010) at sub-solidus temperatures. Oxidation in the liquid state during deceleration is also suggested by the location of metal beads as off-centre objects within most particles, due to migration by settling under the significant deceleration experienced during atmospheric entry (Love and Brownlee, 1991; Yada et al., 1996; Genge, 2016). Oxidation will, however, occur throughout deceleration, even before melting of the precursor metal grain, however, its rate will increase throughout heating as the particle penetrates to lower altitudes as described by Genge (2016).

The observation that thin-films of iron-oxide cover metal beads that are close to the surface of I-types (Figs. 2c, g and 7e, f) suggests that iron-oxide liquid,

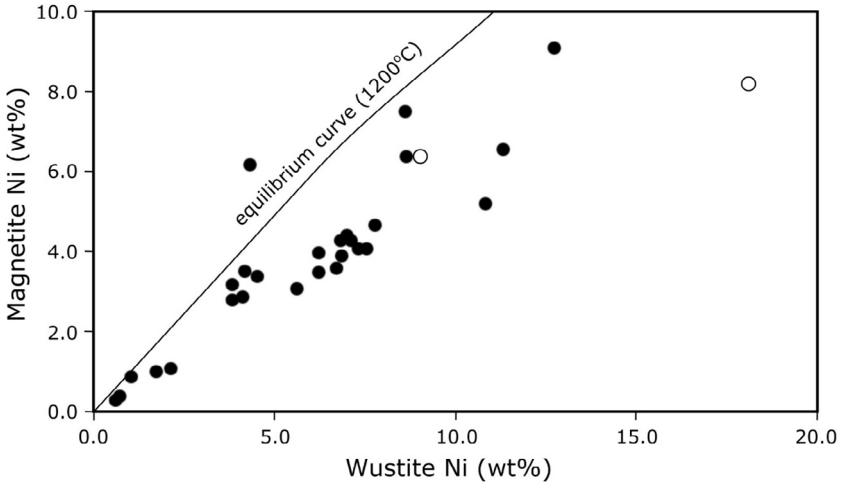

Fig. 15. The Ni content of coexisting magnetite and wüstite within OX spherules. The open symbols show values measured within transitional spherules. The equilibrium partitioning curve at 1200°C is derived from subsolidus Fe-Ni-O phase relations (Raghavan, 2010).

generated by oxidation, wets the surface of the metal. This is consistent with the relative surface tensions of iron metal and iron oxide liquids as discussed by Genge (2016) and implies that oxidation occurs through addition of oxygen to the oxide liquid rather than directly from the atmosphere to the metal liquid. Given that the oxide liquid wets the surface of the metal bead, it suggests that direct evaporation does not occur from the metal, only from the oxide mantle, contrary to the numerical model of Yada et al. (1996) in which only metal evaporation was considered.

Significant additional oxidation of FeNi metal during the sub-solidus portion of flight, after cooling from peak temperature, can be discounted by the smooth nature of the oxide-metal interface in most particles (Fig. 2a–g) and their homogeneous compositions. Experimental studies on solid FeNi steels show the inward diffusion of the highly noble Ni through the solid metal alloy to produces enhanced Ni contents at the metal-oxide interface due to the low diffusion rate of Ni within solid iron metal (Brabers and Birchenall, 1958; Boggs, 1972). Diffusive instability also results in interpenetration of oxides and FeNi steel in experiments due to preferential oxide growth in Ni-poor areas. The homogeneous compositions and smooth nature of metal beads within particles, therefore, indicates minimal low-temperature concentration of Ni by late-stage oxidation. Those spherules in which metal penetrates the surrounding oxide shell (Fig. 7h and i) are, furthermore, distinguished from growth of an oxide rim (termed scale) on solid metal, which has an irregular interface, and instead suggest penetration of liquid metal between solid crystals of wüstite.

Significant evaporation of I-types has occurred during their atmospheric entry with mass losses of up to ~85% identified through Fe and Ni isotope fractionation (Herzog et al., 1999; Engrand et al., 2005). Models of atmospheric entry of I-types indicate that evaporation increases with particle size and entry angle, consistent with isotope fractionation measured in large spherules (Engrand et al., 2005), but suggest that the oxide liquid mantle is not entirely removed by mass loss (Genge, 2016). Relative fractionation of Fe from Ni within large I-types has, however, been shown to be variable with a maximum relative mass fractionation of ~20%. Changes in the Fe/Ni ratio of I-types owing to evaporation are, therefore, relatively minor even though absolute mass loss is large. Oxygen accreted from the atmosphere, however, will experience significant loss by evaporation limiting its availability and its ability to oxidise metal.

4.2. Mineralogical and textural evolution of I-types

The mineralogies and textures of I-types can be explained by the progressive nature of oxidation of liquid metal during entry heating. The Fe-O binary is shown in Fig. 16 and explains the largely bimodal nature of textural types. At temperatures above 1450 °C, a field of liquid immiscibility between metal liquid and oxide liquid (with a composition approximately equivalent to wüstite) occurs between 0 and ~51 atomic % oxygen (0–77 wt% Fe). I-type spherules that accrete less than ~51 atomic % oxygen from the atmosphere during the high temperature portion of their deceleration will, therefore, contain both immiscible liquid metal and liquid oxide producing MET spherules dominated by metal beads and wüstite. Particles that accrete more than ~51% oxygen, in contrast, will retain no metal at chemical equilibrium and instead consist entirely of wüstite and/or magnetite and thus produce OX spherules.

4.2.1. MET Spherules

The Fe-O phase diagram at low oxygen contents is consistent with the overall mineralogy of MET spherules since these particles are dominated by wüstite and FeNi metal. The presence of minor magnetite in MET spherules as dispersed equant grains within the wüstite shells (Fig. 2; Fig. 7c) represents a non-equilibrium assemblage and probably originates by additional, minor sub-solidus oxidation. The rare occurrence of trails of magnetite crystals within

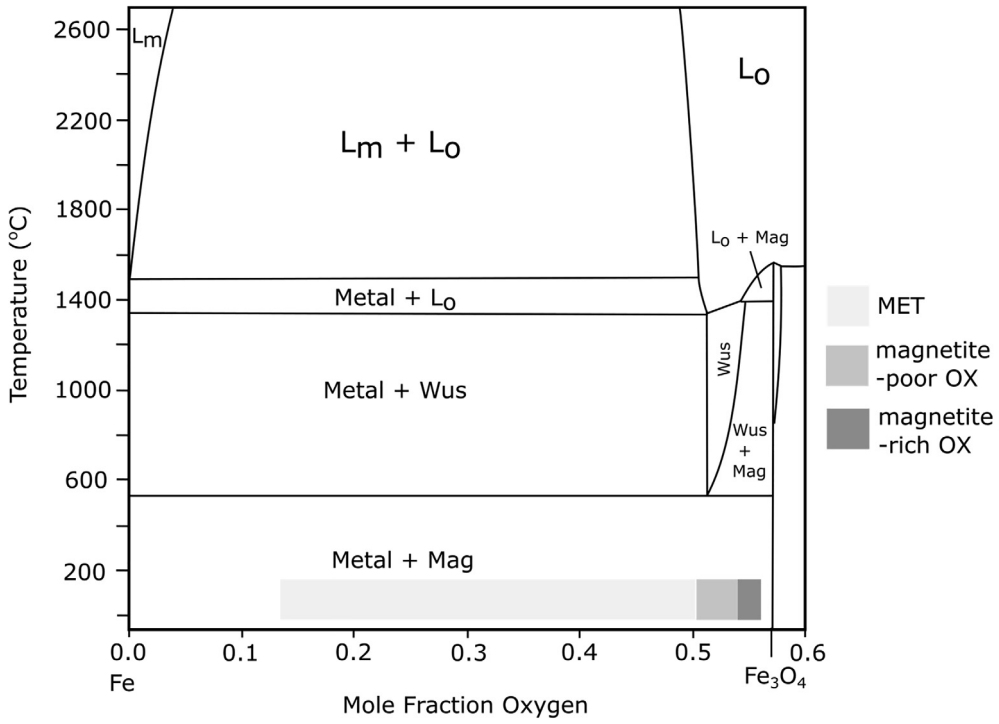

Fig. 16. Phase relations within the Fe-O system (Darken, 1946). The bulk compositional range of MET, magnetite-poor and magnetite-rich OX spherules are shown. Abbreviations: Mag – magnetite, Wus – wüstite, Lm – liquid metal, Lo – liquid oxide.

wüstite (Fig. 7c) suggests growth by grain boundary diffusion of oxygen – known to be important in the solid state oxidation of steels (Appannagaari and Basu, 1995). The irregular nature of the inner margin of magnetite rims on some particles also suggests their growth in the solid state (Fig. 7c and f).

The form of metal within some MET spherules as re-entrant beads, which penetrate between surrounding oxide crystals, is not consistent with either Fe-O or Fe-Ni-O phase relations. The occurrence of metallic protrusions from the bead suggest these form by extrusion and are not simply pockets of metal isolated during oxidation (Fig. 7h and i). Re-entrant beads exhibit extrusions of liquid metal from the bead between dendritic crystals of wüstite, clearly indicating the presence of liquid metal and solid wüstite. This behaviour is contrary to the Fe-O and Fe-Ni-O phase relations that dictate solidification of metal at >1425 °C and crystallisation of wüstite at 1377 °C. Smooth metal beads (Fig. 2a–d), in contrast, are compatible with the phase relations since they are consistent with the solidification of metal prior to wüstite during cooling. The origin of this dichotomy is likely to be due the effects of minor elements on the solidification temperatures of the metal since there is no systematic difference in Ni content between smooth and re-entrant metal beads.

Carbon, sulphur and phosphorous can suppress the liquidus temperature of metal to explain the presence of molten metal with solid wüstite (Kullerud et al., 1969; Okamoto, 1990; Okamoto, 1992). The presence of a few percent carbon with sulphur, furthermore, leads to liquid immiscibility at higher temperatures (Corgne et al., 2008) and complex behaviour. Carbides, sulphides and phosphides are associated with metal within meteorites (Buckwald, 1975; Shibata, 1996; Krot et al., 1997; Brearley and Jones, 1998; Goodrich et al., 2013) and could thus be present within small inclusions in the precursor metal grains. Phosphorous in metal is likely to form phosphate inclusions during oxidation, which were not observed in the studied I-types. Sulphur and carbon, in contrast, are likely to degas during oxidative heating leaving no residual phases. Sulphur contents >10–30 wt% (Kullerud et al., 1969) and carbon contents of >2 wt% (Okamoto, 1992) could decrease the solidification temperature of the metallic liquid below that of wüstite.

The mechanism by which metal liquid is extruded into the surrounding wüstite also needs to be considered. Several mechanisms could be proposed such as the inwards growth of wüstite into liquid metal or the drawing of liquid metal between wüstite crystals by capillary action. The inwards growth of wüstite crystals would require an increase in volume of the oxide liquid on crystallisation to generate an over-pressure on the metal liquid to inject it between the oxide crystals. Increase in volume on crystallisation is more typical of materials with polar molecules or network structures than oxides (Ubbelohde, 1978). Iron-nickel metal liquid also contracts on cooling (Nasch and Manghnani, 1998; Feng et al., 2005) precluding extrusion of metallic liquid by expansion.

Formation of metal veins by drawing of metallic liquid into the narrow spaces between wüstite crystals through capillary action is will be strongly resisted by pressure due to the enclosed nature of the metal bead. In addition

injection by capillary action requires a low contact angle (<60°) between the liquid and solid. Measurements of the contact angle of Fe-Ni alloy liquids on alumina reveal angles >90° (Sharan and Cramb, 1997), which considering the similar surface energies of alumina (2.13–3.5 J m^{-2}; Tepesch and Quong, 2000) and wüstite (3.6 J m^{-2}; Navrotsky et al., 2010) suggests that liquid metal cannot inject into wüstite by capillary action.

A more likely extrusion mechanism for metal extrusion is suggested by particle LK06-0278, which contains a lenticular smooth cavity within its metal bead implying the presence of a gas phase (Fig. 7i). Oxidative degassing of a volatile-bearing component, such as carbide or sulphide, and expansion of produced gas; would cause an overpressure that would extrude metallic liquid into the surrounding wüstite. The presence of finite C, S and/or P element abundances in the precursors of re-entrant MET spherules could, therefore, explain both the solidification temperatures and provide a mechanism for extrusion and thus seems highly likely. The absence of detectable S or P within particles would necessarily require degassing to be a highly efficient process. Carbon cannot be detected using the techniques employed and its presence could not be determined.

4.2.2. OX Spherules

The Fe-O binary system (Fig. 16) predicts that spherules that accrete more than ~51 atomic % oxygen during atmospheric flight will experience complete oxidation of the metallic liquid and form liquid droplets consisting entirely of iron oxides, except for minor amounts of PGE- or Ni-dominated metal. The mineralogical evolution of this liquid on cooling will depend on its oxygen content as shown in Fig. 17. At abundances of <54% atomic % oxygen the liquid will crystallise as wüstite at the liquidus. In contrast at >54% oxygen the liquid will first crystallise magnetite, followed by crystallisation of the residual oxide liquid as wüstite at the solidus. Wüstite crystallised from the iron oxide liquid, however, has an excess of oxygen and thus exsolves magnetite on cooling. Wüstite also becomes metastable at temperatures <570 °C and at equilibrium decomposes at the pro-eutectoid to magnetite and FeNi-alloy (e.g. Young, 2008; Krzyzanowski et al., 2010). However, given the rapid quenching experienced by micrometeorites, the progress of sub-solidus exsolution will be restricted, allowing the survival of wüstite and limiting the exsolution of magnetite.

Magnetite-poor spherules have oxygen contents suggesting that wüstite should crystallise at the liquidus with sub-

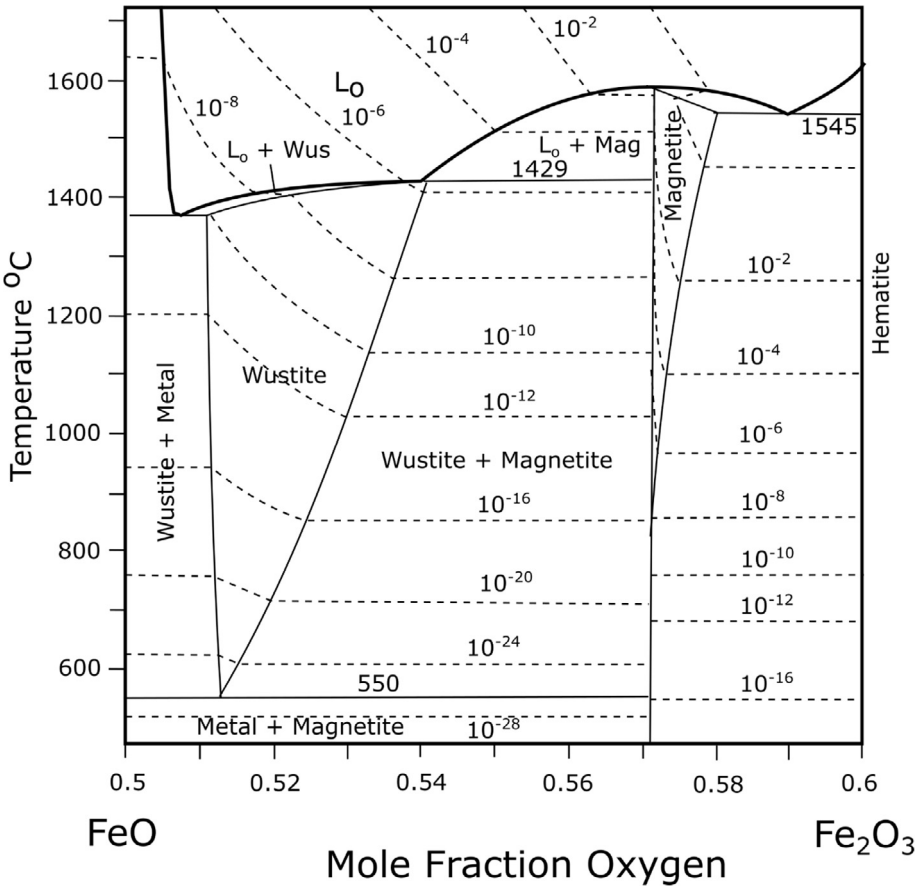

Fig. 17. Detailed phase relations for OX spherules also showing tie lines of constant oxygen fugacity in log units. Notice that pairs of phases buffer oxygen fugacity. Phase diagram was calculated using the thermodynamic package FactSage. Note that minor differences exist to experimentally derived phase relations such as the temperature of the pro-eutectoid at 550 instead of 570 °C. The hematite stability field occurs on the high oxygen margin of the diagram.

sequent sub-solidus exsolution of fine-crystals of magnetite. The occurrence of fine magnetite dendrites within magnetite-poor OX spherules (Fig. 9), however, is apparently contrary to phase relations since dendrites typically would be expected to form by crystallisation from a liquid under large supercooling (Donaldson, 1976). Several features of the magnetite dendrites within the OX particles are, however, unusual. Firstly the magnetite dendrites frequently form radiating clusters oriented at ~120° to each other (Fig. 9a–c) as well as at the 90° intersection that might be expected as a consequence of their spinel structure. Veins of magnetite also occur within the wüstite groundmass of OX spherules and are closely related to the locations of magnetite dendrites (Fig. 9g). The veins are clearly not formed by crystallisation from liquid and suggest sub-solidus nucleation of magnetite along thin cavities. The most likely explanation to reconcile the phase relations and the unusual features of dendrites is that if these crystals form by solid state decomposition of wüstite, with preferential nucleation of magnetite occurring along grain boundaries between pre-existing wüstite crystals that were formed at higher temperature from the liquid. Similar control on magnetite orientation by pre-existing wüstite has furthermore been observed during oxidation of steels (West et al., 2005).

A model for the growth of dendritic crystals in the solid state is shown in Fig. 18 in which lobes of magnetite grow outwards from grain boundaries of pre-existing wüstite crystals. The formation of lobes is suggested to occur due to the diffusion of Ni away from the growing magnetite crystals which gives rise to variable Ni contents within the surrounding wüstite. Preferential growth into Ni poor areas, as observed in experimental oxidation of Ni-bearing steels (Brabers and Birchenall, 1958; Boggs, 1972), results in lobe growth. The presence of small equant crystals of magnetite within wüstite interstitial to dendrites also is likely to occur by decomposition of wüstite. Equant crystals are depleted adjacent to dendrites probably due to depletion of oxygen by growth of the magnetite dendrites.

Several pieces of evidence support the formation of magnetite dendrites in the solid state by growth of lobes perpendicular to wüstite grain boundaries. Most convincing is the occurrence of dendrite morphologies on the external surface of I-types that differ in scale and orientation to the magnetite dendrites within the spherule, suggesting these are surface expressions of the original wüstite crystals formed by crystallisation of the iron oxide liquid (Fig. 12g and h). Magnetite dendrites indeed can be seen in some particles aligning along the grain boundaries of the original wüstite dendrites (Fig. 12h). The occurrence of radiating magnetite clusters at 120°, representing triple junctions between the original wüstite crystals, is also consistent with this explanation. The presence of cavities aligned along grain boundaries of wüstite dendrites in OX spherules (Fig. 3c), which are otherwise unobservable within backscattered electron images, is further evidence that such wüstite crystals exist in these particles and predate the formation of the magnetite. The composition of these spherules, estimated from their wüstite and magnetite abundances, also fall in the field of liquidus wüstite crystallisation. The observation of linear, bifurcating cavities close to the centre of well-developed magnetite dendrites in particle LK06-0924 (Fig. 9c and e) further supports magnetite formation by decomposition of wüstite and nucleation on grain boundaries. Finally, although the formation of magnetite dendrites in the solid state may seem contrary to the limited time of the heating pulse which is of the order a 2–20 of seconds, self-diffusion coefficients for oxygen within wüstite are relatively high ($\sim 10^{-5}$ cm^2 s^{-1} at 1390 °C; Krzyzanowski et al., 2010), owing to its high vacancy density, allowing lobes of a few microns in width to form within such short periods.

The enhanced abundance of magnetite dendrites near the surface of some low-magnetite OX spherules suggests that late stage oxidation also plays a role in development of I-type textures. Continued oxidation of spherules after solidification is predicted by models of atmospheric entry since their cooling rates are decreased by continued heating by ongoing deceleration (Genge, 2016). Observation of trails of magnetite crystals within some MET spherules (Fig. 7c), furthermore, indicates their formation by grain boundary diffusion. Because oxidation and cooling are surface processes, and temperature controls the rate of diffusion, the late stage formation of magnetite is concentrated at the surface and along grain-boundaries explaining the surface correlated abundance of magnetite in many spherules (Fig. 3a, d, f; Fig. 7f; and Fig. 11a).

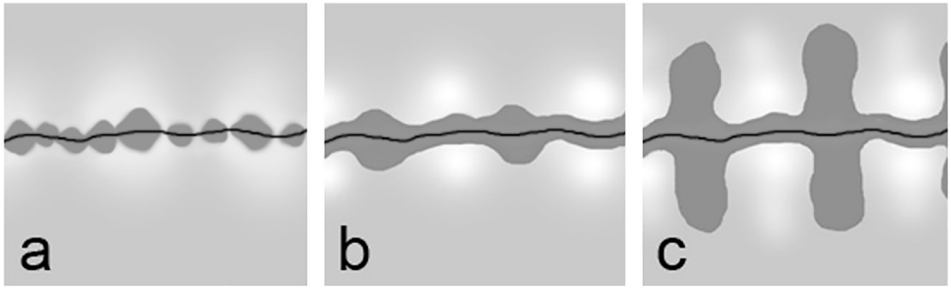

Fig. 18. Model for the formation of magnetite dendrites within OX spherules. (a) Magnetite (dark grey) initially nucleates on grain boundaries between wüstite (light grey) forming trails of magnetite crystals. (b) Diffusion of Ni away from the growing magnetite into the wüstite results in variable Ni-abundance along the surface (light areas are Ni-rich) with preferential growth of lobes in Ni-poor areas. (c) Continued preferential growth in Ni-poor areas produces dendrites of parallel lobes.

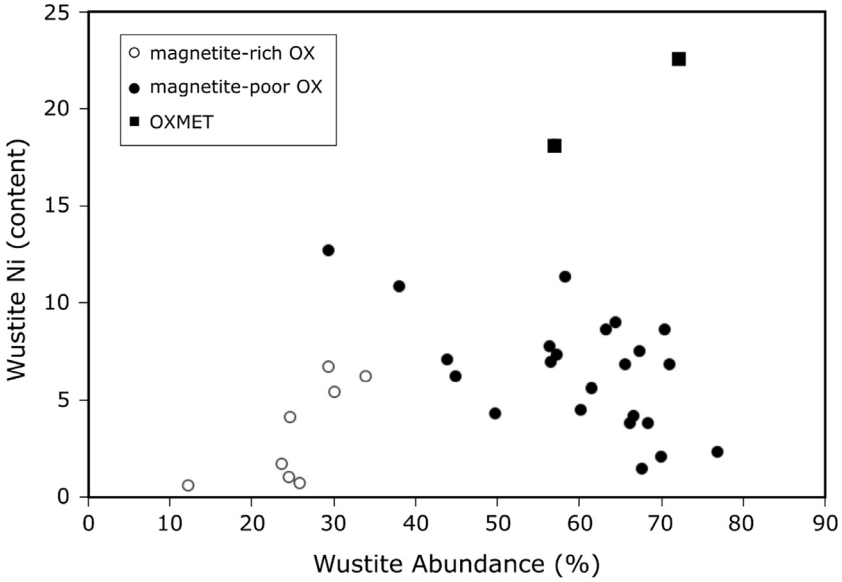

Fig. 19. Wüstite Ni content against wüstite abundance within OX and OXMET spherules.

Magnetite-rich OX particles have bulk compositions that fall within the region of liquidus magnetite crystallisation (Fig. 17). The coarser grain-size of their magnetite crystals (Fig. 3) is consistent with their crystallisation at higher temperature from a liquid rather than in the solid state, since their growth rate in the liquid is enhanced by higher diffusion rates. Although both OX types exhibit increases in dendrite width with particle diameter, magnetite-rich OX spherules have larger crystal widths at a given particle size than magnetite-poor OX particles indicating different conditions of crystallisation for the two types (Fig. 6). Similarly the Ni content of wüstites within magnetite-poor OX particles broadly increases with magnetite abundance (and thus decreasing wüstite abundance), consistent with non-equilibrium diffusion of Ni into wüstite during solid state growth of magnetite. Wüstites within magnetite-rich OX particles, in contrast, exhibit a separate trend (Fig. 19).

Given magnetite crystallisation from the liquid oxide within magnetite-rich OX spherules, the different crystal habits observed may relate to cooling rate with equant crystals forming at lower cooling rate than dendritic crystals. Variations in crystal habit due to peak temperature, which influences crystal morphology by nuclei destruction (Donaldson, 1976), are unlikely since the different mineralogy of the precursor prior to oxidation is unlikely to provide suitable nuclei.

4.2.3. OXMET I-types

OXMET I-types have non-equilibrium mineral assemblages with metal beads surrounded by rims of wüstite within shells containing magnetite dendrites (Fig. 11). The occurrence of metal together with relatively abundant magnetite implies significant spatial variation of oxygen fugacity of several orders of magnitude can be developed within some spherules when metal abundances are small. All OXMET spherules have mantles of magnetite-free wüstite surrounding smooth metal beads suggesting that the wüstite nucleated on the surface of the metal. Additional oxidation of the remaining oxide liquid during crystallisation might explain their spatially variable oxygen contents.

4.3. Evolution of phase chemistry

The mineral chemistries within I-type spherules are broadly consistent with Fe-Ni-O phase relations (Fig. 20). The phase relations predict that wüstite in equilibrium with metal in MET spherules should contain less than 1.0 wt% Ni whilst coexisting with metal containing less than 67 wt % Ni. During progressive oxidation the Ni content of metal beads increases by preferential partitioning of Fe into the oxide liquid whilst the more noble Ni is retained in the metal as previously noted by Brownlee (1985). This process will continue until the metal liquid is completely consumed. If no other losses of Fe or Ni occurred, then the oxide liquid would have the same Ni/Fe ratio as the original metal grain.

Fig. 14 shows the composition of wüstite and coexisting metal within MET spherules compared with the equilibrium values derived from the Fe-Ni-O ternary at 1500 °C. Wüstite Ni contents are generally lower than the equilibrium predictions. Observations of Ni-enrichment of metal adjacent to growing oxide scales during high temperature oxidation of steels (Boggs, 1972) indicate a kinetic influence on wüstite-metal Ni partitioning. Nickel is enhanced in the metal phase due to its inwards diffusion ahead of the oxidation front. The degree of divergence from equilibrium may relate to differences in the rate of oxidation as well as temperature and cooling rate. Metal compositions within beads are, however, largely homogeneous with differences of <1 wt% Ni and thus must have equilibrated during cooling. Metal extruded into surrounding wüstite mantles in dendritic MET spherules, however, do exhibit higher Ni con-

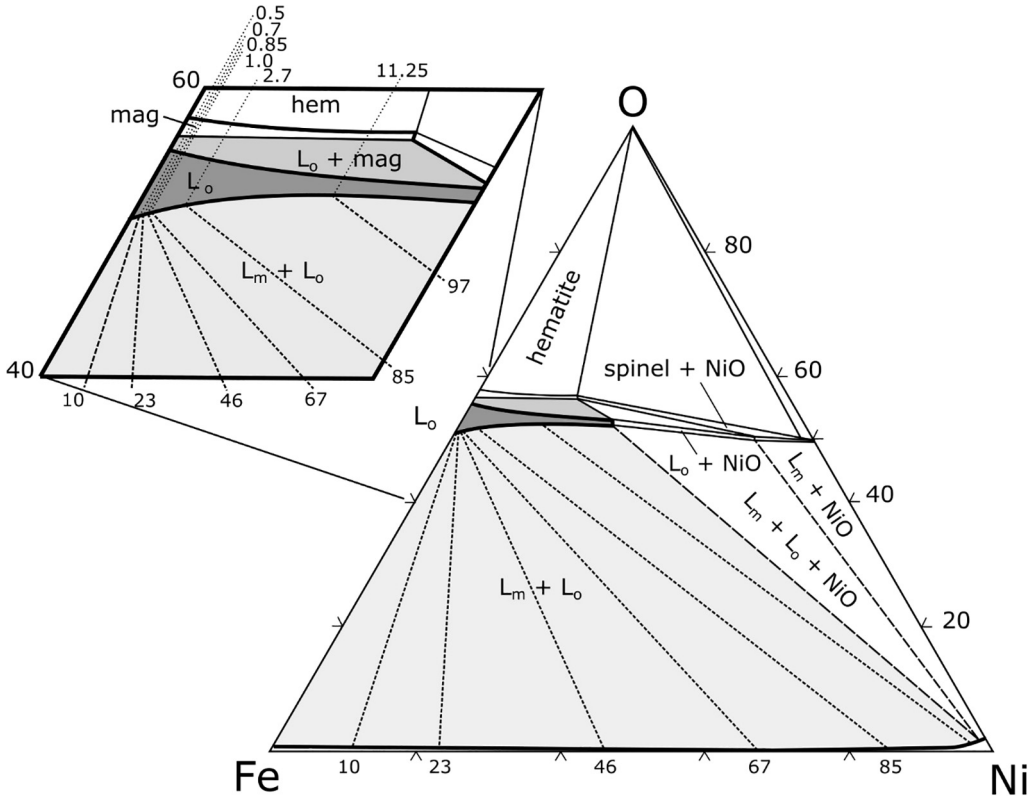

Fig. 20. Phase relations in the system Fe-Ni-O system at 1500 °C (Raghavan, 2010). Tie lines show the compositions of coexisting liquid metal (Lm) and liquid oxide (Lo).

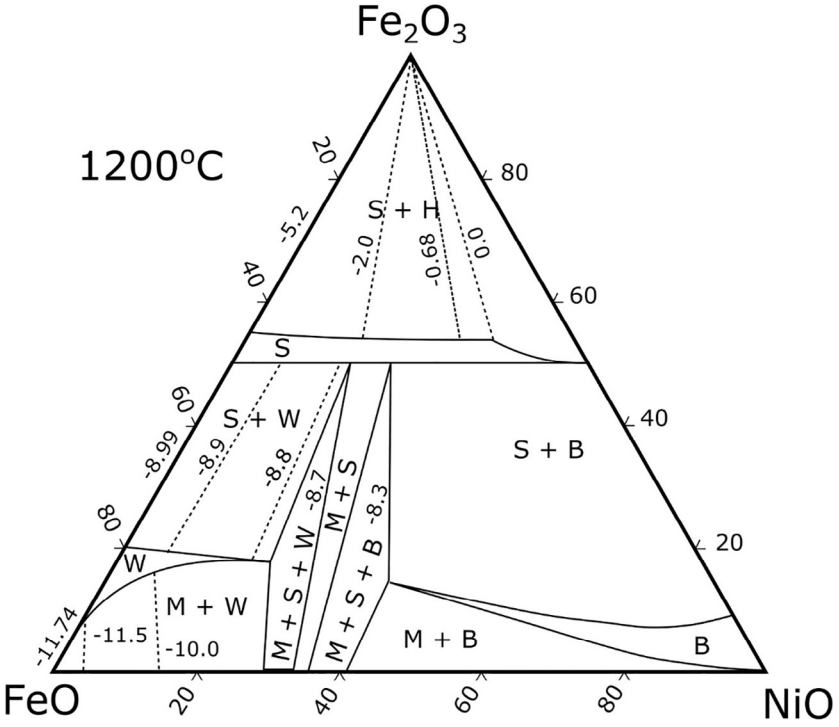

Fig. 21. Phase relations in the system Fe-Ni-O at 1200 °C (Raghavan, 2010). Tie lines show the compositions of coexisting phases and are oxygen fugacity buffers in units of log fO_2. Abbreviations: magnetite (spinel structure S), wüstite (W), hematite (H), bustenite (B) and metal (M).

tents than in coexisting metal beads because within these small bodies of metal, Ni enriched areas are less easily diluted by sub-solidus equilibration.

The Fe-Ni-O sub-solidus phase relations (Fig. 21) also provide constraints on the compositions of coexisting magnetite and wüstite within OX spherules shown in Fig. 15. Wüstite and magnetite compositions change with oxygen fugacity with higher Ni content at higher values (log fO_2 −8.99 to −8.7 at 1200 °C). Wüstite in OX spherules has higher Ni content relative to magnetite compared with the equilibrium values predicted by the phase relations. Non-equilibrium behaviour is, however, likely in the solid state, in particular considering the short duration of the heating pulse during atmospheric deceleration. The significantly higher self-diffusion coefficients within wüstite compared with magnetite (Krzyzanowski et al., 2010) would predict Ni enrichment of wüstite under rapid cooling as observed. Diffusive instabilities resulting in variable Ni enrichment of wüstite along the interface with the growing magnetite was suggested above to result in the preferential growth of magnetite into areas of lower Ni-wüstite resulting in lobate scale interfaces (Fig. 18). The divergence from equilibrium behaviour may provide a proxy for sub-solidus cooling rate.

4.4. Magnetite rims and late stage oxidation

Discrete magnetite rims are developed on the external surface of both MET and OX particles (Figs. 2 and 3) and probably form by solid state oxidation during cooling rather than either the preferential crystallisation of a magnetite shell on the surface of a molten particle, or non-oxidative solid state exsolution from wüstite. Surface crystallisation of the liquid on cooling is unlikely since thermal gradients are minimal within particles of these dimensions (Love and Brownlee, 1991). Non-oxidative solid state exsolution of magnetite at the surface of the particle isn't consistent with the presence of magnetite rims on MET particles and would also result in the exsolution of metal alloy. Formation by further oxidation on cooling in the solid state is thus the most likely scenario since during cooling the particle will have penetrated to lower altitudes where fO_2 is higher.

The formation of magnetite rims in the solid state, by oxidation of underlying wüstite, is suggested by the presence of wüstite inclusions in some magnetite rims on low-magnetite OX particles (Fig. 3d). Rim magnetite within these particles envelopes magnetite dendrites already formed by sub-solidus decomposition of wüstite and must, therefore, be formed at lower temperature. Studies of solid state oxidation of metals reveal that wüstite dominated scale layers grow at temperatures greater than 570 °C and are ~20 times wider than magnetite layers (Chen and Yuen, 2003). Magnetite formation in scales on steel is thought to be impeded by the lower diffusion rate of oxygen within magnetite than in wüstite and to be principally driven by outwards diffusion of iron through wüstite (Young, 2008; Krzyzanowski et al., 2010). Areas of wüstite within the magnetite rim on I-types, therefore, can be preserved if they are protected from outwards iron diffusion by magnetite dendrites. This will also decrease the growth rate of the magnetite rim overlying isolated inclusions of wüstite. Localised control of magnetite rim growth may also explain their somewhat variable Ni contents.

The growth of magnetite rims at sub-solidus temperature is also strongly suggested by the presence of lenticular magnetite rims in direct contact with metal within some MET spherules (Fig. 7g). Oxidation experiments on steel indicate that at temperatures of >570 °C metal oxidizes to wüstite with an outermost layer of magnetite, whilst at temperatures <570 °C steel oxidizes directly to magnetite (Young, 2008; Krzyzanowski et al., 2010). The occurrence of penetrative magnetite rims on metal beads, therefore, indicates that minor low temperature oxidation occurs at a late stage in the thermal pulse, most likely in those spherules with low cooling rates. The formation of such rims after entry heating by oxidation on the Earth's surface can, furthermore, be discounted since such weathering observed in the current study is dominated by hydrous iron oxides such as ferrihydrite (Fig. 7j) and alteration to magnetite is not observed on metal within silicate micrometeorites (Genge and Grady, 1998; Genge, 2005; Genge et al., 2008; Van Ginneken et al., 2016).

Given that magnetite rims form at sub-solidus temperatures, their widths might be expected to vary depending to the cooling rate of spherules. The maximum width of magnetite rims broadly increases with particle diameter (Fig. 10), albeit with a significant scatter. Models of the entry heating of I-types demonstrate that cooling rate decreases with the diameter of particles allowing greater time for growth of the magnetite rim (Genge, 2016). Dependence of rim growth on other parameters, such as the partial pressure of oxygen at the external surface of the particle and internal control of oxygen fugacity by mineral buffers, probably explains the wide range of magnetite rim thicknesses observed between spherules of a similar size.

Variation in the growth of magnetite rims as a result of the external pO_2 is suggested by observations of variable development of magnetite rims within individual particles. Within MET spherules magnetite rims are often wider on the side of the spherule containing the off-centre metal bead (Fig. 2c and 7f). The position of the metal bead is the result of migration under the influence of deceleration (Yada et al., 1996; Genge and Grady, 1998) and thus indicates the flight direction of the particle (e.g. Sauvet et al., 2011). Atmospheric oxygen atoms are encountered by the leading face of the particle resulting in higher pO_2 and thus the enhanced growth of the magnetite rim. Engrand et al. (2005) furthermore identifies a good correlation between $\delta^{17,18}O$ composition and the thickness of the magnetite rim implying rim growth is directly related to the degree of heating and thus peak altitude and oxygen partial pressure.

Enhanced abundances of equant dispersed magnetite in MET particles towards the edge of the particle within the wüstite shell are also observed in some MET spherules (Fig. 7c). Observations that the abundance of dispersed equant magnetite grains in wüstite shells decreases adjacent to well-developed magnetite-rims, however, implies that some outwards diffusion of iron also occurs. Oxygen avail-

ability, particularly in the later stages of I-type formation is complex and not necessarily directly equivalent to the pO_2 of ambient atmosphere since it is influenced by particle orientation and partly buffered by existing mineral assemblages.

4.5. Cavities and degassing

The occurrence of irregular, smooth cavities, comprising up to 10 vol% of particles (Fig. 3), particularly within OX I-types, suggests that a gas phase was present within I-types during entry heating. Previous studies have suggested several mechanisms for the presence of voids including the removal of metal by weathering or separation (Genge et al., 1997), the inwards crystallisation of wüstite dendrites, and the presence of a gas phase (Feng et al., 2005).

Removal of metal by weathering most likely explains the presence of spherical voids with similar sizes and locations to metal beads (Fig. 2j). Most commonly such voids are contained within wüstite dominated particles and some contain ferrihydrite formed by alteration of metal (Fig. 2i). Irregular voids, in contrast, must have a different origin since they have distinctly different outlines to metal beads, and none contain the weathering products of metal.

Inwards crystallisation of wüstite dendrites into the liquid oxide might result in central cavities owing to the smaller specific volume of wüstite compared to the oxide liquid resulting in contraction of the oxide shell (Feng et al., 2005). The formation of voids through contraction, however, will be strongly resisted by pressure unless a gas phase is present to fill the void space. In the absence of a gas phase the remaining liquid is likely to be drawn into the region rather than leave a vacuum.

Irregular voids usually have shapes tracing intergranular areas between dendrites (Fig. 3c and e) and are common in OX particles (88% of OX spherules). Using microtomography Feng et al. (2005) showed that cavities often form cylindrical volumes through the centre of particles and suggested they form by concentration of gas towards the rotational axis of rapidly spinning particles, indicating the presence of gas whilst particles were molten. This scenario is compatible with studies on the spin-up of micrometeorites during entry heating (Genge, 2017) and strongly implies that a gas phase was present whilst the particle was partially liquid.

Feng et al. (2005) proposed oxygen or hydrogen as a possible gas phase. Oxygen gas has previously been observed filling lenticular cavities within the oxidation scales on steel and accumulates due to heterogeneous migration of oxygen by grain boundary diffusion at sub-solidus temperatures (Brabers and Birchenall, 1958; Krzyzanowski et al., 2010). A similar lenticular cavity that might represent sub-solidus accumulation of oxygen was observed in OXMET I-type LK06-0678 (Fig. 11a) which exhibits enhanced sub-solidus magnetite growth adjacent to the cavity. Excess oxygen gas within OX particles at supra-solidus temperatures is unlikely due to the intermediate oxygen contents of these wüstite-dominated particles. Sulphur dioxide or CO_2 generated by oxidative heating of sulphide and/or carbide present within the precursor particle is perhaps more likely given the frequent intimate association of metal and these phases in meteorites (Buckwald, 1975; Shibata, 1996; Krot et al., 1997; Brearley and Jones, 1998; Goodrich et al., 2013). Mineral inclusions present within metal grains would be expected to melt, given the high peak temperatures experienced by these particles (>2000 °C; Genge, 2016). Tomkins et al. (2013), for example, show that chromite + metal melts in achondritic meteorites at temperatures >1050°C. Finite Cr contents within wüstite and magnetite observed in some particles likely represent melted chromite inclusions, although, as discussed previously by Herzog et al. (1999), they might also represent Cr-bearing precursor metal compositions.

Volatile-bearing minerals such as troilite (FeS) and cohenite (Fe_3C) would degas rapidly during the oxidative heating of atmospheric entry. Within silicate micrometeorites sulphide degassing has been proposed as the primary mechanism for vesicle generation (Taylor et al., 2011). The occurrence of cavities within some I-types may, therefore, be consistent with the presence of a volatile-bearing component. The precursors of I-types may, therefore, not be simple single phase metal grains but multi-phase assemblages dominated by FeNi metal.

Particle LK06-0278 (Fig. 7i) provides support for the presence of a gas phase associated specifically with the metal in I-types. The expansion of the gas vesicle within the metal bead in this particle provides a mechanism for the extrusion of metal from beads into the grain boundaries between the surrounding wüstite dendrites. If extruded metal is due to the presence of gas vesicles then a sulphide or carbide component could be relatively common since 23% of MET spherules exhibit metal extrusion. A larger proportion of OX spherules (88%), however, contain cavities suggesting they have different precursors or more of their volatile components have been liberated from metal into the gas phase by oxidation. The observation that MET and OX particles form textures compatible with progressive oxidation, which is principally controlled by entry parameters (Genge, 2016), is most consistent with enhanced gas production due to oxidation rather than different precursors.

4.6. Formation of Ni-rich and Pt-group nuggets

Platinum group nuggets were observed in 10 spherules in the current study whilst a further 5 contain high Ni metal nuggets with Pt detectable within EDS spectra; sometimes occurring as trails within magnetite-lined veins. Rudraswami et al. (2011) reported similar abundances and occurrences of Pt-group and Ni-rich nuggets within deep-sea I-type spherules from the Indian Ocean. Brownlee et al. (1984) suggested that Pt-group nuggets form by the complete oxidation of FeNi metal beads through retention of the highly noble PGEs within a residual metallic nugget. This model is consistent with the occurrence of large PGE-rich, Ni-bearing nuggets, several microns in size

observed in many studies (Brownlee et al., 1984; Bonte et al., 1987; Feng et al., 2005; Rudraswami et al., 2011). The observation that a single large PGE-nugget tends to occur close to margin of spherules is consistent with their formation by direct oxidation of the metal phase which likewise migrates toward the surface during deceleration because of its higher density. No large PGE-nuggets were observed in the current study, however, their presence cannot be excluded since plane of section effects make their detection difficult.

Bonte et al. (1987) and Rudraswami et al. (2011) both noted that numerous sub-micron PGE-rich nuggets occur within some I-types, mostly contained within magnetite crystals. Bonte et al. (1987) suggested that two separate processes are required to explain the formation of large and small PGE nuggets. Rudraswami et al. (2011, 2014) noted the presence of Ni-rich PGE-bearing nuggets in I-types, similar to those identified here, sometimes within trails and suggested these evolve into sub-micron PGE nuggets by further oxidation. Analyses of nuggets by Rudraswami et al. (2011) indicate that sub-micron nuggets are enriched in volatile PGEs and thus not consistent with oxidative heating.

In this study sub-micron PGE nuggets were observed only within magnetite-rich OX spherules, whilst Ni-rich PGE-bearing nuggets were observed in both magnetite-rich and magnetite-poor OX spherules. Nuggets were observed mainly within magnetite crystals (Fig. 9h) except those dispersed along magnetite-rich veins (Fig. 9g). Nickel-rich PGE-bearing metal was observed in the most abundance associated with symplectic intergrowths with magnetite at the interface with wüstite (Fig. 9e and f) indicating formation by solid state decomposition of wüstite at grain boundaries. The Fe-O phase relations suggest the formation of symplectites occurs at the pro-eutectoid at temperatures <570°C. The same textures are observed in scales on slow cooled steels (Chen and Yuen, 2003) and thus imply unusually low cooling rates for these spherules. Trails of PGE-bearing nuggets within magnetite veins might also have a similar origin. The enrichment observed in volatile PGEs measured by Rudraswami et al. (2011) is consistent with their formation by decomposition since the PGE contents will be dependent on partitioning coefficients between magnetite and metal rather than volatility.

Sub-micron PGE-rich nuggets within coarse-magnetite crystals in magnetite-rich OX spherules are problematic since these crystals formed by crystallisation at the liquidus. Exsolution of PGE-rich metal directly from magnetite would not be expected since PGEs are likely to be concentrated within the residual wüstite liquid rather than the early magnetite. Trapping of wüstite inclusions within liquidus magnetite crystals followed by decomposition of wüstite at lower temperatures is probably the most likely explanation for these isolated sub-micron PGE-rich nuggets in these spherules, in particular since trapped iron oxide liquid inclusions will have significant oxygen excesses and thus will readily decompose. Sufficiently high PGE contents within wüstite may require the complete oxidation of metal prior to the formation of magnetite – consistent with the observation that PGE-nuggets were not observed within MET or OXMET I-types.

4.7. Separation of metal beads and particle bulk compositions

The separation of metal beads during atmospheric entry as a consequence of the large decelerations experienced by spherules has been proposed previously and is consistent with the observation that metal beads migrate to the leading face of spherules (Brownlee and Bates, 1983; Bonte et al., 1987; Yada et al., 1996; Herzog et al., 1999; Engrand et al., 2005). The separation of remnant beads will cause losses of the most noble elements that preferentially partition into metal, such as Ni, Co and PGEs. The low Ni contents of wüstite and magnetite in some I-types have been previously suggested to indicate that this process has a major effect on the bulk compositions in particles (Herzog et al., 1999).

The observation that most MET spherules have low-Ni wüstite (<1.5 wt% Ni) and most OX spherules have high-Ni wüstite and magnetite has significant implications for metal separation. Low-Ni wüstite in MET spherules is consistent with near equilibrium with metal, rather than metal loss; although metal separation is possible after significant equilibration. The lack of metal beads within 26% of MET spherules also does not necessarily imply these particles have lost metal by separation since it is broadly consistent with plane-of-section discovery rate for off-centre beads. Furthermore, two MET spherules lacking metal beads have external ferrihydrite rims suggesting they contained metal out of the plane of section that has been partially or completely weathered (Van Ginneken et al., 2016). The high-Ni wüstite and magnetite within OX spherules, in contrast, dictates either complete oxidation of metal or loss of only a small residual Ni-rich metal bead.

Whether separation occurs from OX spherules or whether these are formed by complete oxidation of metal can be investigated comparison of the bulk compositions of MET and OX spherules; assuming both to sample the same precursor population. Estimating bulk compositions from phase chemistry, however, is fraught with difficulty due to plane of section effects on the relative abundance of phases, as highlighted in previous studies (e.g. Kyte, 1983). In the current study the cross-sectional area of metal beads and oxide mantles was used to estimate bulk composition assuming the beads are spherical and that the oxide mantle is a hemispherical shell comprising the remaining volume of the particle. For any particular bead the measured area is most likely to be lower than the true value and thus compositions give minimum estimates for Ni abundance. Compositions estimated for OX spherules dominated by wüstite and magnetite are likely to be much more accurate since they are based simply on the cross-sectional area of magnetite and wüstite crystals.

Fig. 22 shows the calculated Ni/Fe ratios of spherules. Metal-bead free (OX) spherules have a restricted range and average lower Ni/Fe ratios than MET spherules suggesting that metal separation has depleted their Ni contents. No estimate can be given for the proportion of metal separated from spherules from this data alone since the Ni-content of metal at the time of separation is unknown.

The Ni content of metal coexisting with the oxide shell, can be calculated by mass balance if it is assumed

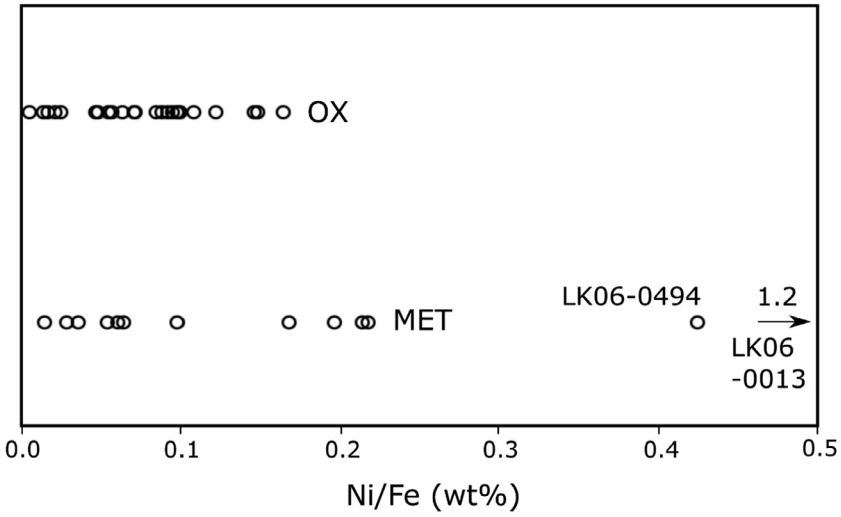

Fig. 22. Bulk Ni/Fe calculated from apparent abundances of metal, magnetite and wüstite for OX and MET spherules. Metal bead-bearing spherules (MET) have higher average Ni/Fe than OX spherules. Two MET spherules (LK06-0494 and LK06-0013) have significantly higher Ni/Fe ratios.

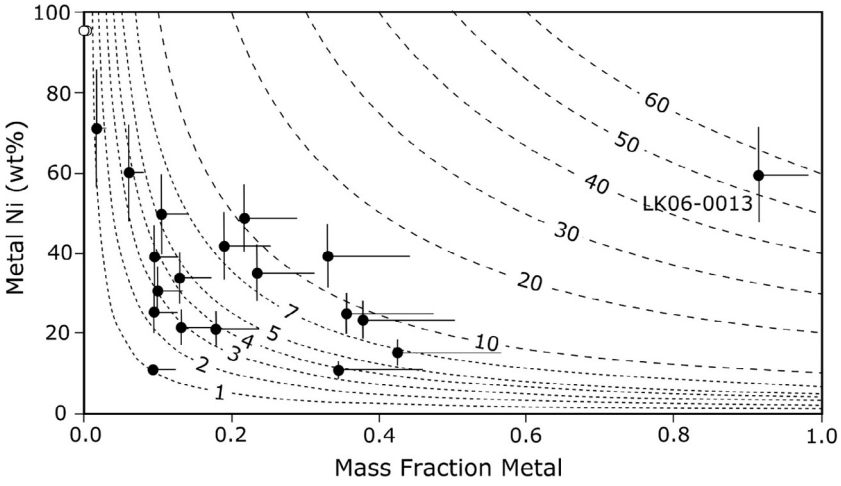

Fig. 23. Ni content of metal compared with mass fraction of metal within particles. The dashed lines represent the paths of metal evolution with progressive oxidation assuming mass balance and no evaporative Ni/Fe fractionation. The original composition of precursor metal grains is shown at a mass fraction of metal of 1.0, with increasing oxidation Fe preferentially partitions into the growing oxide mantle resulting in an increase in the Ni content of the remaining metal. Error bars show an example 20% error in mass fraction of metal, due to plane of section effects, and a 20% variation in Ni contents due to evaporation.

that no Ni and Fe fractionation occurs due to partial evaporation. The mass fraction of metal observed within spherules compared with its calculated and observed Ni content is shown in Fig. 23 with dashed lines representing the fractionation of Ni between coexisting metal and oxide assuming negligible oxide Ni content. Ignoring inaccuracies in metal abundance measurements, the data imply that the majority of particles were derived from precursors with low Ni contents, broadly in the range of kamacite, although one particle (LK06-0013) is demonstrably derived from a high Ni precursor, presumably taenite.

Predicting the effect of Ni/Fe fractionation due to evaporation is difficult due to lack of experimental data in the liquid state. Studies of the isotopic compositions of I-type spherules, however, indicate a wide range of evaporative loss for iron of 30–85% by mass (Herzog et al., 1999; Engrand et al., 2005) and thus suggest evaporation could play an important role in compositional evolution. Isotopic measurements, however, are only available for spherules significantly larger in size than those studied here and modelling of I-types indicate that degree of evaporative loss increases dramatically with particle size (Genge, 2016). Herzog et al. (1999) measured both Fe and Ni mass fractionation and showed that evaporative loss of Ni could be up to 20% larger or smaller than for Fe. This value is used here to define error bars for the Ni content of metal and suggests relatively little effect.

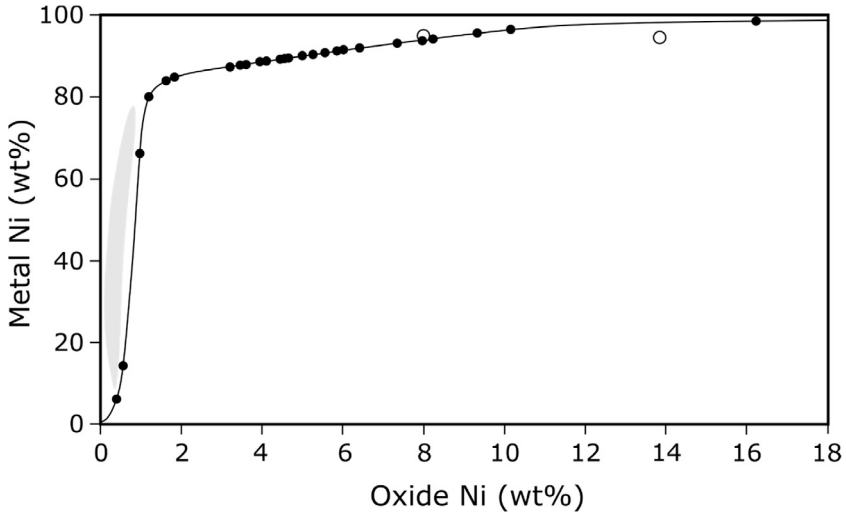

Fig. 24. Composition of metal in equilibrium with wüstite within OX spherules. The equilibrium curve is derived from Fe-Ni-O phase relations at 1500 °C (Raghavan, 2010). The shaded area shows compositions of low-Ni wüstite in MET spherules. Solid symbols show the predicted metal compositions for OX spherules. Open symbols show the measured metal and wüstite Ni contents in OXMET.

One independent means to estimate the Ni content of metal beads on separation is to consider the Ni abundance within wüstite in metal-free (OX) spherules. I-type spherules form by the oxidation of liquid metal, consequently these particles must have contained metal beads earlier in flight which have either been completely oxidized or have been lost by separation. Assuming equilibration between coexisting oxide and metal liquids at the point of separation, the Ni abundance of wüstite can be used to estimate the metal composition given Fe-Ni-O phase relations and suggest metal Ni contents of >80 wt% for all but two spherules (Fig. 24). Given that in MET spherules wüstite has lower Ni contents than expected at equilibrium, the Ni content of separating metal may have been higher than this estimate; a suggestion supported by the small residual beads within OXMET spherules that contain up to 95 wt% Ni. Comparison with Fig. 23 allows an estimate of the mass fraction of metal at separation, assuming that the precursor composition was kamacite, and gives values of <0.2. Whether most of the metal beads that were present within OX spherules during heating separated or were completely oxidized remains difficult to conclusively assess. The presence of Pt-group nuggets within some OX I-types, however, suggests complete oxidation did occur in some cases since these elements would have been sequestered into metal and lost during separation (Brownlee et al., 1984).

The shapes of metal beads and host spherules reveal how metal separation can occur. Particles in which metal beads are close to the surface, and thus near separation, often exhibit non-spherical particle and bead shapes; suggesting surface tension interactions. Where metal beads are close to the surface they are often oblate with their short axes aligned in the direction of flight (Fig. 2c). Similarly particles containing near-surface, small metal beads (<0.4 particle diameter) tend to have pits of lower curvature closest to the metal bead (Fig. 2d). Where the metal bead is almost exposed at the surface, and thus is close to separation, the pit is often concave with only a thin-veneer of oxide over the bead (Fig. 7e).

Genge (2016) discussed the influence of surface tension on the separation of metal beads and argued that since oxide liquids wet the surface of liquid metal, surface tension will strongly resist bead separation. Thin-veneers of oxide on near-surface metal beads in I-types indicate that such wetting occurs. The separation of a metal bead, therefore, is most likely when the bead is small allowing a higher interfacial angle with the oxide liquid. Separation necessarily involves the withdrawal of iron oxide liquid from the region between the metal bead and the surface under the influence of the interaction of surface tensions as illustrated in Fig. 25. The observed deformation of metal beads and spherules is thus likely to have occurred as a result of oxide liquid film withdraw and indicates that in some spherules metal bead separation was close to occurring.

Although it is not possible to determine the fraction of I-type particles that have experienced metal bead separation, beyond a maximum of ~50% (OX I-types), the results suggest that separated metal droplets will be small in comparison to the original spherule and contain high Ni contents of >80 wt%. To date such metallic particles have not been found amongst micrometeorite collections, however, they are likely to be susceptible to weathering.

4.8. Sources of I-type cosmic spherules

Identifying the parent bodies of the metallic precursors of I-type spherules is complicated by the effects of oxidation and evaporation on the composition of individual phases and the effects of evaporation and metal separation on bulk compositions. Herzog et al. (1999) reconstructed the bulk compositions of I-type spherules using isotopic measurements of Fe, Ni and Cr to constrain mass fractionation by evaporation and concluded that the majority of I-type cosmic spherules are derived from Cr-bearing metal similar

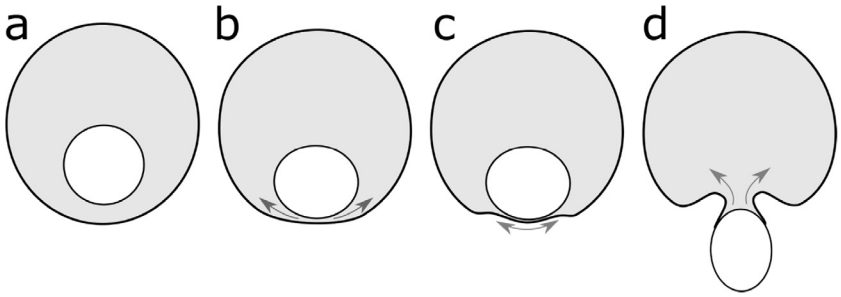

Fig. 25. Model showing mechanisms of metal droplet separation. (a) Liquid metal bead approaches leading face of spherule in direction of motion due to deceleration. (b) Interaction between surface tensions of the outer surface and metal-oxide liquid interface deform the spherule and the metal bead causing flow of liquid oxide out of the meniscus. (c) Thinning of the meniscus of oxide liquid occurs due to flow. (d) Separation of the bead occurs by a thinning neck of oxide liquid which still wets the metal bead.

to that in CM, CR and CV chondrites, rather than ordinary chondrites or iron meteorites. Herzog noted that the small size of metal grains within these meteorites presents a problem in generating large I-type cosmic spherules. Genge (2016) suggested that bulk Cr contents within ordinary chondrite derived metal grains might be elevated by the presence of chromite inclusions in the precursor and suggested that the abundance of I-types was consistent with the abundance of metal in these meteorites and the constraints provided by silicate micrometeorites on the relative abundance of materials from ordinary and carbonaceous chondrite sources. In the current study 22 particles have detectable Cr within oxide phases suggesting these were derived from Cr-bearing metal grains or had precursors containing chromite inclusions. Chromium is detected in metal in only one particle, presumably due to its efficient partitioning into the oxide liquid. The maximum wüstite Cr-content observed of 1.57 wt% (LK06-0937) is higher than observed within chondrite metal (Herzog et al., 1999) and thus is likely to indicate the presence of a chromite inclusion within the precursor. Bulk compositions, as discussed above, also suggest the majority of particles had precursors with low Ni contents of 1–10 wt% consistent with kamacite, although particle LK06-0013 appears to have a taenite precursor.

The Ni/Co ratios of metal beads are likely to be relatively diagnostic of the precursor due to the similar oxidation behaviour of these elements. Measurements of Ni/Co ratio within extruded metal are equivalent to those of coexisting metal beads, despite their elevated Ni contents, supporting minimal fractionation of these elements during oxidation subsequent to extrusion. Values of Ni/Co ratio in most metal beads vary from 14 to 35. The lowest observed Ni/Co ratios are in the range of kamacite from H-group and unequilibrated ordinary chondrites (Affiatalab and Wasson, 1980), but are larger then those of from kamacite within L and LL-group ordinary chondrites and type 3 carbonaceous chondrites (Fuchs and Olsen, 1973; Affiatalab and Wasson, 1980). The majority of metal beads have Ni/Co ratios in the range of CM and CR chondrite kamacite, and one is also similar to that of CB metal (Campbell et al., 2002). Cobalt was not detected in the Ni-rich metal bead within particle LK06-0013 which considering detection limits suggests Ni/Co ratios of >100, compatible with taenite within most chondrites and achondrites. Iron meteorites have highly variable Ni/Co ratios due to exchange between kamacite and taenite and chemical zoning with kamacite varying between ~8 and 30 whilst taenite has values ~45 to 180 (Goldstein et al., 2014), thus Ni/Co ratio cannot distinguish between chondritic and iron meteorite sources.

The chemistry of metal beads in I-types, together with consideration of changes in absolute Ni content due to oxidation, suggests that most precursors are derived from CM, CR, H, or iron meteorite kamacite with rare particles derived from taenite. Previous studies of bulk composition by Herzog et al. (1999) suggested the bulk Cr contents are most compatible with CM, CR and CV chondrites, but are too high for iron meteorite metal, and emphasise the difficulties of evaluating compositional fractionation by evaporation. The nature of the precursors, however, is complicated by the potential for multi-phase assemblages. Sulphides, carbides and chromite are intimately associated with metal in chondrites, achondrites and iron meteorites (Buckwald, 1975; Shibata, 1996; Krot et al., 1997; Goodrich et al., 2013) and could change bulk compositions sufficiently to make their parent body associations elusive.

Re-entrant metal beads suggest sulphide or carbide within the precursors of 23% of MET spherules that have been lost by degassing during oxidative heating. Sulphides are intimately associated with metal in chondritic meteorites whilst carbides are rare (e.g. Brearley and Jones, 1998); whereas carbides are intimately associated with metal as plessite within iron meteorites (Buckwald, 1975). The identity of the volatile-bearing phase within I-types thus depends on their source. The high Cr in wüstite in at least one particle suggests the presence of chromite in the precursor. Silicates might also have been present within precursors, particularly those from chondritic sources. The presence of palagonite interstitial to dendrites in MET spherules could be interpreted as altered silicate glass, however, absence of unaltered glass within any spherule, despite the preservation of glassy silicate spherules at Larkman Nunatak, implies the palagonite gel is precipitated during weathering. Similar precipitates were observed by van Ginneken et al. (2016) in silicate micrometeorites and further emphasise that bulk compositions can be biased by weathering. As discussed by Genge (2016) and Herzog

et al. (1999) metal grain sizes and abundances make irons, stony-irons, CB and H-chondrites the most suitable sources for I-types, although CR chondrites can also contain metal grains of sufficient size to generate particles <200 μm in diameter.

5. IMPLICATIONS

5.1. Identifying I-type spherules in the geological record

I-type cosmic spherules have been recovered from a wide range of sedimentary rocks and provide a sample of the Earth's extraterrestrial dust flux throughout geological time (Taylor and Brownlee, 1991; Dredge et al., 2010; Onoue et al., 2011; Voldman et al., 2013; Tomkins et al., 2016). The resistance of iron oxides to weathering and diagenesis, combined with the ready separation of I-types by magnetic techniques makes these particles particularly useful in studies of ancient micrometeorites. The oldest I-types discovered to date were recovered from Archean limestones and have been used to demonstrate that the upper atmosphere in the Archean had elevated oxygen abundances, contrary to expectation (Tomkins et al., 2016).

Reliable identification of ancient I-type spherules is a crucial part of studies of cosmic dust from the geological record. Several criteria can be proposed on the basis of observations made in this paper and previous works (e.g. Taylor and Brownlee, 1991; Dredge et al., 2010; Onoue et al., 2011; Tomkins et al., 2016) for the positive identification of I-types: (i) spherical particle morphologies, (ii) dendritic crystal habits, (iii) Ni-bearing wüstite and magnetite, (iv) the presence of void spaces, either after dissolution of metal by weathering, or due to degassing during flight, (v) the presence of FeNi metal, and (vi) the presence of a variety of MET, OXMET and OX type particles.

5.1.1. Spherical particle morphologies

Spherical particle morphologies are perhaps the least conclusive criteria. The majority of I-types have a large degree of sphericity due to their formation as liquid droplets compared to terrestrial iron oxide grains in this size range including wind-blown sand and diagenetically produced magnetite framboids (Suk et al., 1990). Biogenically produced magnetite furthermore occurs at significantly smaller sizes of <1 μm although larger clusters of these grains can approach the size of I-types (Chang and Kirschvink, 1989).

5.1.2. Dendritic crystals

The occurrence of dendritic oxide crystal morphologies on spherical particles, either on the surface or within polished sections is, however, particularly characteristic of I-types since it results from their formation by crystallization of liquid droplets under rapid cooling, although in homogeneous MET spherules dendrites are not evident. Given the high melting temperatures of oxides (>1300°C) there are few magmatic processes that could generate liquid iron oxide microspherules, in particular, without substantial lithophile (Mg, Al, Mn and Si) materials. Magnetite-rich spherules with equant crystals may, however, resemble diagenetic framboids (Suk et al., 1990). Impact spherules, resulting from the collision of larger meteoroids with the Earth's surface, can also have spherical shapes and dendritic magnetite morphologies of I-types, although most contain appreciable silicate materials (Glass and Simonson, 2013). Criteria other than spherical shape and dendrite occurrence are thus required for positive identification.

5.1.3. Ni-bearing wüstite and magnetite

The presence of abundant wüstite is one criterion that distinguishes I-type spherules from other extraterrestrial-related sources. Impact spherules and meteorite ablation spherules (generated during atmospheric entry of meteorites) form at low altitude under higher oxygen fugacities than I-type cosmic spherules, which are generated during the high altitude deceleration of metallic extraterrestrial dust. Magnetite is, therefore, abundant within impact spherules (Glass and Simonson, 2013; Folco et al., 2015), and is likely to be abundant within meteorite ablation spheres (Genge and Grady, 1999; Van Ginneken et al., 2010; Badyukov and Raitala, 2012), whilst wüstite is abundant within the majority of I-type cosmic spherules. Only minor wüstite (<5%) was observed in meteorite ablation spherules associated with the fall of the Sikhote Alin iron meteorite (Badyukov and Raitala, 2012) and may be present in small amounts in iron oxide impact spherules associated with the Kamil crater in Egypt which was likewise formed by an iron meteorite projectile (Folco et al., 2015). That minor wüstite is associated with impact and meteorite ablation spherules means that the most magnetite-rich I-types may not be easily distinguished these spherules even though they appear to have subtly different textures. Impact spherules and meteorite ablation spherules are, however, much rarer than I-types since the extraterrestrial flux of cosmic spherules is significantly higher than that of larger meteoroids with a surface flux of ~1600 t/a compared to ~10 t/a of meteorites (Love and Brownlee, 1993; Taylor et al., 2000; Bland et al., 1996). Iron meteorites also comprise only 4.4% of recovered meteorites (data from the Meteoritical Bulletin). Abundance of spherules, however, is a poor criterion considering impact and ablation spherules can be abundant at a single locality, and impact spherules can have global distribution for large events, albeit one that is stratigraphically restricted. Iron oxide dominated impact spherules are, nevertheless, largely associated with smaller impact craters formed by iron projectiles and are only locally significant (e.g. Folco et al., 2015).

Terrestrial wüstite occurrences include orthomagmatic Ni-sulphide deposits, such as Disko Island, where basaltic melts have undergone significant reduction by carbon (Mariano et al., 2012). In such materials wüstite contains no detectable Ni and is intimately associated with graphite, cohenite (Fe_3C), sulphides and low-Ni iron metal (Bird et al., 1981), none of which is observed within I-types. Wüstite can also occur as a rare component within some carbonate bearing skarns and related hydrothermal veins where it is thought to form by reduction of other iron-rich phases and is intimately associated with siderite, magnetite, galena, sphalerite and silicates (Nadoll and Mauk,

2011). The compositions of hydrothermal wüstite are often Mn-bearing. Other examples of wüstite are less abundant. It has been described within thermally metamorphosed coal associated with magnetite and siderite (Ciesielczuk et al., 2015) and is present as rare inclusions with diamond (Kaminsky et al., 2009). Of terrestrial occurrences those of orthomagmatic deposits are most similar to that of I-type cosmic spherules but are unlikely to be widely abundant except in the vicinity of such deposits.

Survival of wüstite within I-types is also worthy of consideration since it is metastable at low temperatures. Decomposition of wüstite to magnetite and metal alloys might occur over geological timescales. The recent discovery of wüstite-bearing I-type spherules from 2.7 Ga limestones in Pilbara, Australia (Tomkins et al., 2016); however, demonstrates its long term survival given suitable conditions. Magnetite is likewise metastable at low temperature and can be oxidised to maghemite (Zhou et al., 2001), or altered during reductive diagenesis to pyrite particularly in marine sediments (Rowan et al., 2009). Pristine magnetite has been reported within Archean, Ordovician and Triassic fossil micrometeorites (Dredge et al., 2010; Onoue et al., 2011; Tomkins et al., 2016). Alteration was implied due to lithophile element contents within Jurassic cosmic spherules (Taylor and Brownlee, 1991), however, the presence of silicate precipitates between magnetite crystals reported here might also explain the presence of lithophile elements within I-types.

The Ni-contents of magnetite and wüstite within I-types are an important criterion. All studied particles contained Ni contents in wüstite >0.1 wt% with Ni contents up to 22.5 wt% observed within OXMET spherules. The presence of Ni-bearing dendritic wüstite, with or without magnetite, in spherules represents very strong evidence for an extraterrestrial origin since this element has not been observed in magnetite framboids (Suk et al., 1990). Observations of iron oxide meteorite ablation spherules and impact spherules, however, reveal similar ranges of oxide Ni content to I-types, but exhibit a smaller range of Ni/Co ratios in addition to the large abundance of magnetite (Badyukov and Raitala, 2012; Folco et al., 2015). The absence of Ni within magnetite and wüstite, however, may not exclude an extraterrestrial origin since compositional change during diagenesis might occur.

5.1.4. FeNi metal

Metallic FeNi with Ni contents of 10 to 95 wt% are characteristic of MET I-type spherules and together with the presence of abundant dendritic Ni-bearing wüstite in spherical particles constitute conclusive evidence for an origin as cosmic spherules. Metallic FeNi is very rare on Earth occurring within rare orthomagmatic deposits, reduced basalts (Searle, 1958; Bird et al., 1981) and serpentinites (Nickel, 1959), although the Ni/Co ratios within these examples differ from chondritic values. Metallic FeNi is also observed within some meteorite ablation and impact spherules but is present in much smaller proportion of particles than in I-types (Badyukov and Raitala, 2012; Folco et al., 2015). Metal would, however, be expected to have a low preservation potential within ancient I-types recovered from sediments and yet has been observed as small dispersed metal grains, similar to those formed by extrusion from metal beads, within Archean I-types (Tomkins et al., 2016) and within Triassic micrometeorites (Onoue et al., 2011). Removal of metal by weathering is nevertheless observed in many Antarctic I-type spherules producing spherical off-centre cavities (Van Ginneken et al., 2016) and metal was not preserved in spherules recovered from Jurassic hardgrounds by Taylor and Brownlee (1991). The presence of spherical voids, together with other criteria, is good evidence for the original presence of metal beads.

5.1.5. Textural type

Finally, the textural diversity I-types is also evidence for an origin as extraterrestrial dust and is an inescapable consequence of the variation of entry angles even for a single entry velocity population since this causes variable oxidation (Genge, 2016). In a collection of I-types recovered from sediments MET, OX and OXMET spherules should all be present. Some variation in mineral abundances and textures in ancient I-types might, however, be expected owing to different atmospheric oxygen contents (Tomkins et al., 2016), atmospheric density profiles and the entry velocity of dust particles.

5.2. Entry parameters of I-type spherules

The properties of I-types can be related to their entry parameters. The degree of oxidation of metal increases with particle size and entry angle owing to deceleration at lower altitude under higher partial pressures of oxygen (Genge, 2016). Metal is consequently rarely preserved within spherules >300 μm in diameter (Brownlee et al., 1984) and the magnetite to wüstite ratios of OX spherules increase with particle size. Rare large spherules up to 650 μm in diameter containing metal (Engrand et al., 2005) can therefore be identified as those that entered the atmosphere at low entry angles (<20°). Conversely small metal free spherules (<100 μm) are most likely to have entered the atmosphere at high angle or may have experienced separation of metal droplets. The observed range of metal bead sizes compared to particle size, furthermore, falls largely within the range predicted by Genge (2016) for a low entry velocity population (Fig. 8). The Ni-content of precursor metal grains, however, decreases oxidation rate and thus enhances metal survival. The observation that particle LK06-0013 has an anomalously large, Ni-rich metal bead for its size is thus consistent with its formation from a Ni-rich taenite precursor.

Several textural features may allow atmospheric entry parameters to be further constrained. Cooling rates decrease with particle size (Genge, 2016) consistent with the observation that dendrite widths increase with size of the particle (Fig. 6). Dendrite width is likely to depend on cooling rate since crystal growth rate is largest at high temperatures and rapid cooling thus limits the opportunity for growth. Cooling rate, however, also increases with entry angle and may explain why dendrite widths show a range of values at any particular particle size since those with the highest entry angles having cooled quickest and have

the least opportunity for dendrite growth. Magnetite rims show an increase in width with particle size that may be dependent on cooling rate (Fig. 10). The degree of disequilibria of wüstite and magnetite compositions, conversely is likely to be largest at the highest cooling rates. Magnetite rim widths and disequilibria in phase compositions, however, also have a dependence of the pO2 which is partly controlled by the altitude of deceleration and consequently have less direct relevance to cooling rate. Exsolution of Ni-rich metal symplectic intergrowths, as a result of decomposition of wüstite at the pro-eutectoid are observed in only a few particles and may be an indicator of exceptionally low cooling rate. These are most likely to be low entry angle particles.

6. CONCLUSIONS

Observations of 88 I-type cosmic spherules recovered from moraine at Larkman Nunatak in Antarctica reveal a wide variety of textures and mineral assemblages that testify to their formation by melting and progressive oxidation of extraterrestrial FeNi metal grains during atmospheric entry. Forty-seven percent of I-types are metal bead-bearing (MET) spherules that form under relatively low degrees of oxidation (<51 atomic % oxygen) at supra-liquidus temperatures corresponding the two liquid field between metallic and oxide liquids in Fe-Ni-O phase diagram. The remaining I-types form after complete oxidation, or after removal of remnant metal beads, to generate metal bead-free OX spherules dominated by wüstite and magnetite. Where supra-liquidus oxidation is intermediate (<54 atomic % oxygen) magnetite-poor OX spherules form by crystallisation of non-stoichiometric wüstite at the liquidus followed by subsolidus decomposition to form magnetite dendrites by grain boundary nucleation. At higher degrees of oxidation magnetite-rich I-types form by crystallisation of coarse magnetite at the liquidus. Sub-solidus oxidation of spherules during cooling occurs to generate equant magnetite crystals within MET spherules and additional dendrites close the surface of OX spherules. Magnetite rims are found on most spherules and are often best developed on the leading face of particles due to enhanced pO_2 and are suggested to form by sub-solidus oxidation. Symplectic assemblages of Ni-rich metal and magnetite are observed in some particles, together with magnetite-lined veins sometimes containing trails of Ni-rich, Pt-bearing metal nuggets, and are probably formed by decomposition of wüstite at temperatures <570 °C. Sub-micron PGE-rich nuggets are mainly observed within magnetite-rich OX spherules and are suggested to form by decomposition of wüstite inclusions. The compositions and mass fractions of metal beads in MET spherules, together with the Ni contents of OX spherules, demonstrate that separation of metal from particles occurs during deceleration. Separated metal beads in most particles are, however, inferred to be limited to mass fractions of <0.2 and have Ni contents of >80 wt%. The precursor dust grains of I-type cosmic spherules are suggested on the basis of Ni/Co ratios and the evolution of Ni contents with the mass fraction of metal to be consistent mainly with kamacite grains, although a single particle with a taenite precursor was identified. The Ni/Co ratio also suggests that H-group and unequilibrated ordinary, CM, CR, CB and iron meteorite parent bodies are possible. The presence of iron sulphides or carbides within the precursors of 23% of MET spherules is suggested by the presence of vesicles in metal and their lower melting temperatures. The occurrence of chromite inclusions within precursors is implied by finite Cr-contents within 22 spherules. The abundance of MET spherules and the increase in OX spherule abundance with size are shown to be consistent with a low entry velocity population of dust (12 km s^{-1}) whilst dendrite width compared with particle size is suggested as a proxy for entry angle due to the effect on cooling rate. The following criteria are recommended for the conclusive identification of I-type spherules within sediments and sedimentary rocks: (i) spherical particle morphologies, (ii) dendritic crystal morphologies within wüstite and magnetite dominated particles, (iii) the high abundance of wüstite, (iv) Ni-bearing wüstite and magnetite, and (v) the presence of relict FeNi metal. The similarity between I-types and meteorite ablation and impact spherules derived from iron meteorites requires detailed characterisation of mineralogy and texture in order to distinguish them.

ACKNOWLEDGEMENTS

This work was supported on by the Science and Technology Council (STFC) [grant number ST/J001260/1]. The paper was written by the lead author with data collected by Genge, Davies, Van Ginneken and Suttle. All authors contributed to review and discussion of content. Greg Herzog is acknowledged for his many insightful comments on this manuscript in his role as editor. Three reviewers, including Cecile Engrand are thanked for their useful comments.

REFERENCES

Affiatalab F. and Wasson J. T. (1980) Composition of the metal phases in ordinary chondrites: implications regarding classification and metamorphism. *Geochim. Cosmochim. Acta* **44**, 431–446.

Anselmo A. (2007) Observations of false spherical micrometeorites. arXiv: 0708.4276.

Appannagaari N. and Basu S. (1995) Modelling of O-18 tracer distribution during double oxidation – experiments for inward growing scales. *J. App. Phys.* **78**, 2060–2069.

Badyukov D. D. and Raitala J. (2012) Ablation spherules in the Sikhote Alin meteorite and their genesis. *Petrologiya* **20**, 574–582.

Bird J. M., Goodrich C. A. and Weathers M. S. (1981) Petrogenesis of Uivfaq iron, Disko Island, Greenland. *J. Geophys. Res.* **86**, 11787–11805.

Bi D., Morton R. D. and Wang K. (1993) Cosmic nickel-iron alloy from Pleistocene sediments, Alberta, Canada. *Geochim. Cosmochim. Acta* **57**, 4129–4136.

Blackhurst R. L., Genge M. J. and Grady M. M. (2004) Microbial D/H fractionation in extraterrestrial materials: application to micrometeorites and Mars. Lunar Planet. Sci 35. Lunar Planet. Inst., Houston. #1584 (abstr.).

Blanchard B. B., Brownlee D. E., Bunch T. E., Hodge P. W. and Kyte F. T. (1980) Meteorite ablation spheres from deep-sea sediments. *Earth Planet. Sci. Lett.* **46**, 178–190.

Bland P. A., Smith T. B., Jull A. J. T., Berry F. J., Bevan A. W. R., Cloudt S. and Pillinger C. T. (1996) The flux of meteorites to the Earth over the last 50000 years. *Mon. Not. R. Astron. Soc.* **283**, 551–565.

Boggs W. E. (1972) Gas-metal reactions in mixed environments. In AIME (eds S. A. Jansson & E. A. Foroulis), Boston. pp 1–45.

Bonte P., Jehanno C., Maurette M. M. and Brownlee D. E. (1987) Platinum metals and microstructure in magnetic deep sea spherules. *J. Geophys. Res.* **93**, 641–648.

Brabers M. J. and Birchenall C. E. (1958) High temperature oxidation of iron-nickel alloys. *Corrosion* **14**, 33–36.

Brearley A. J. and Jones R. H. (1998) Chondritic meteorites. In Planetary Materials, Vol. 36 (eds by J. J. Papike). Min. Soc. Amer. pp 1–191.

Brownlee D. E. (1985) Cosmic dust: collection and research. *Ann. Rev. Earth Planet. Sci.* **13**, 147–173.

Brownlee D. E. and Bates B. (1983) Meteor ablation spherules as chondrule analogs. In Chondrules and their Origins (edited by E. A. King, Lunar and Planetary Institute. pp 10–25.

Brownlee D. E., Bates B. A. and Wheelock M. M. (1984) Extraterrestrial platinum group nuggets in deep sea sediments. *Nature* **309**, 693–695.

Buckwald V. F. (1975) *Handbook of iron meteorites, their history, distribution, composition and structure*. Verlag, Univ. California.

Campbell A. J., Humayun M. and Weisberg M. K. (2002) Siderophile element constraints on the formation of metal in the metal-rich chondrites Bencubbin, Weatherford and Gujba. *Geochim. Cosmochim. Acta* **66**, 647–660.

Chang S.-B. R. and Kirschvink J. L. (1989) Magnetofossils, the magnetization of sediments, and the evolution of magnetite biomineralization. *Ann. Rev. Earth Planet. Sci.* **17**, 169–195.

Chen R. Y. and Yuen W. Y. D. (2003) Review of the high-temperature oxidation of iron and carbon steels in air or oxygen. *Oxidation Metals* **59**, 433–468.

Ciesielczuk J., Kruszewski L. and Majka J. (2015) Comparative mineralogical study of thermally-altered coal-dump waste, natural rocks and the products of laboratory heating experiments. *Int. J. Coal Geol.* **139**, 114–141.

Corgne A., Wood B. J. and Fei Y. (2008) C- and S-rich molten allow immiscibility and core formation of planetesimals. *Geochim. Cosmochim. Acta* **72**, 2409–2416.

Davidson J., Genge M. J., Mills A. A., Johnson D. J., and Grady M. M. (2007). Ancient cosmic dust from Triassic salt. 38th Lunar and Planetary Science Conference, Lunar and Planetary Science XXXVIII, Houston. Lunar Planet. Inst. #1338 (abstr.).

Darken L. S. (1946) The system iron-oxygen. II. Equilibrium and thermodynamics of liquid oxide and other phases. *J. Am. Chem. Soc.* **68**, 798–816.

Donaldson C. H. (1976) An experimental investigation of olivine morphology. *Contrib. Min. Petrol.* **57**, 187–213.

Dredge I., Parnell J., Lindgren P. and Bowden S. (2010) Elevated flux of cosmic spherules (micrometeorites) in Ordovician rocks of the Durness Group, NW Scotland. *Scottish J. Geol.* **46**, 7–16.

Engrand C., McKeegan K. D., Leshin L. A., Herzog G. F., Schnabel C., Nyquist L. E. and Brownlee D. E. (2005) Isotopic compositions oxygen, iron, chromium, and nickel in cosmic spherules: toward a better comprehension of atmospheric entry heating effects. *Geochim. Cosmochim. Acta* **69**, 5365–5385.

Feng H., Jones K. W., Tomov S., Stewart B., Herzog G. F., Schnabel C. and Brownlee D. E. (2005) Internal structure of type I deep-sea spherules by X-ray computed microtomography. *Meteorit. Planet. Sci.* **40**, 195–206.

Folco L., D'Orazio M., Fazio A., Cordier C., Antonio Z., van Ginneken M. and El-Barkooky A. (2015) Microscopic impactor debris in the soil around Kamil crater (Egypt): inventory, total mass, and implications for the impact scenario. *Meteorit. Planet. Sci.* **50**, 382–400.

Fuchs L. H. and Olsen E. (1973) Composition of metal in type III carbonaceous chondrites and its relevance to the source-assignment of lunar metal. *Earth Planet. Sci. Lett.* **18**, 379–384.

Genge M. J. (2005) Chondrules in Antarctic micrometeorites. *Meteorit. Planet. Sci.* **40**, 225–238.

Genge M. J. (2008) Koronis dust in antarctic ice. *Geology* **36**, 687–690.

Genge M. J. (2016) The origins of I-type spherules and the atmospheric entry of iron micrometeoroids. *Meteorit. Planet. Sci.* **51**, 1063–1081.

Genge M. J. (2017) Vesicle dynamics during the atmospheric entry heating of cosmic spherules. *Meteorit. Planet. Sci.* **52**, 443–457.

Genge M. J. and Grady M. M. (1998) Melted micrometeorites from Antarctic ice with evidence for the separation of immiscible Fe-Ni-S liquids during entry heating. *Meteorit. Planet. Sci.* **33**, 425–434.

Genge M. J. and Grady M. M. (1999) The fusion crusts of stony meteorites: implications for the atmospheric reprocessing of extraterrestrial materials. *Meteorit. Planet. Sci.* **34**, 341–356.

Genge M. J., Grady M. M. and Hutchinson R. (1997) The textures and compositions of fine-grained Antarctic micrometeorites – implications for comparisons with meteorites. *Geochim. Cosmochim. Acta* **61**, 5149–5162.

Genge M. J., Engrand C., Gounelle M. and Taylor S. (2008) The classification of micrometeorites. *Meteorit. Planet. Sci.* **43**, 497–515.

Glass B. P. and Simonson B. M. (2013) *Distal Impact Ejecta Layers: A Record of Large Impacts in Sedimentary Deposits*. Springer-Verlag, Berlin, pp. 92–118.

Goldstein J. I., Yang J. and Scott E. R. D. (2014) Determining cooling rates of iron and stony-iron meteorites from measurements of Ni and Co at kamacite-taenite interfaces. *Geochim. Cosmochim. Acta* **140**, 297–320.

Goodrich C. A., Ash R. D., Van Orman R. D., Domanik K. and McDonough W. F. (2013) Metallic phases and siderophile elements in main group ureilites: implications for ureilite petrogenesis. *Geochim. Cosmochim. Acta* **112**, 340–373.

Gounelle M., Chaussidon M., Morbidelli A., Barrat J., Engrand C., Zolensky M. E. and McKeegan K. (2009) A unique basaltic micrometeorite expands the inventory of early solar system planetary crusts. *Proc. Natl. Acad. Sci.* **106**, 6904–6909.

Heck P. R., Ushikubo T., Schmitz B., Kita N. T., Spicuzza M. J. and Valley J. W. (2010) A single asteroidal source for extraterrestrial Ordovician chromite grains from Sweden and China: high precision oxygen three-isotope SIMS analysis. *Geochim. Cosmochim. Acta* **74**, 497–509.

Herzog G. F., Xue S., Hall G. S., Nyquist L. E., Shih C. Y., Wiesmann H. and Brownlee D. E. (1999) Isotopic and elemental composition of iron, nickel and chromium in type I deep-sea spherules: implications for origin and composition of the parent micrometeoroids. *Geochim. Cosmochim. Acta* **63**, 1443–1457.

Kaminsky F., Wirth R., Matsyuk S., Schreiber A. and Thomas R. (2009) Nyererite and nahcolite inclusions in diamond: evidence for lower-mantle carbonatitic magmas. *Mineral. Mag.* **73**, 797–816.

Krot A. N., Zolensky M. E., Wasson J. T., Scott E. R. D., Keil K. and Oshumi K. (1997) Carbide-magnetite assemblages in type 3 ordinary chondrites. *Geochim. Cosmochim. Acta* **61**, 219–237.

Krzyzanowski M., Beynon J. H. and Farrugia D. C. J. (2010) *Oxide Scale Behaviour in High Temperature Metal Processing*. Wiley, Weinheim, pp. 35–45.

Kullerud G., Yund R. A. and Moh G. H. (1969) Phase relations in the C-Fe-S, Cu-Ni-S and Fe-Ni-S systems. In *Magmatic ore deposits*, (ed. Wilson H. D. B.). *Econ. Geol. Mono.* **4**, 323–343.

Kyte F. T. (1983) Analysis of exterrestrial materials in terrestrial sediments. Ph.D Thesis. Univ. California.

Larsen J. (2016) *In Search of Stardust*. Arthouse DGB, Oslo, ISBN: ISBN: 978-82-8181-201-7.

Love S. G. and Brownlee D. E. (1991) Heating and thermal transformation of micrometeoroids entering the Earth's atmosphere. *Icarus* **89**, 26–43.

Love S. G. and Brownlee D. E. (1993) A direct measurement of the terrestrial mass accretion rate. *Science* **262**, 550–553.

Mariano G. I., Gaillard F., Scaillet B., Polozo A. G., Marecal V., Pirre M. and Arndt (2012) Extremely reducing conditions reached during basaltic intrusion into organic matter-bearing sediments. *Earth Planet. Sci. Lett.* **357**, 319–326.

Maurette M., Olinger C., Michel-Levy M. C., Kurat G., Pourchet M., Brandstatter F. and Bourot-Denise M. (1991) A collection of diverse MMs recovered from 100 tonnes of Antarctic blue ice. *Nature* **351**, 44–47.

Nasch P. M. and Manghnani M. H. (1998) Molar volume, thermal expansion, and bulk modulus in liquid Fe-Ni alloys at 1 bar: Evidence for magnetite anomalies? In Properties of Earth and Planetary Materials at High Pressure and Temperature (eds Manghnani M. H. and Yagi T.). Geophys. Monogr. Ser., 101, p 307–317, AGU, Washington, D. C.

Nadoll P. and Mauk J. L. (2011) Wüstite in a hydrothermal silver-lead-zinc vein, Lucky Friday mine, Coeur d'Alene mining district, USA. *Am. Mineral.* **96**, 261–267.

Navrotsky A., Ma C., Lilova K. and Birkner N. (2010) Nanophase transition metal oxides show large thermodynamically drive shifts in oxidation-reduction equilibria. *Science* **330**, 199–201.

Nickel E. H. (1959) The occurrence of native nickel-iron in the serpentinite rock of the eastern townships of Quebec province. *Canad. Min.* **6**, 191–199.

Noguchi R., Ohashi N., Tsujimoto S., Takuya M., Mitsunari T., Bradley J. P., Nakamura T., Shoichio T., Stephan T., Naoyoshi I. and Naoya I. (2015) Cometary dust in Antarctic ice and snow: past and present chondritic porous micrometeorites preserved on the Earth's surface. *Earth Planet. Sci. Lett.* **410**, 1–11.

Okamoto H. (1990) The Fe-P (iron-phosphorous system). *Bull. Alloy Phase Diagrams* **11**, 404–412.

Okamoto H. (1992) The C-Fe (carbon-iron system). *J. Phase Equilib.* **13**, 543–565.

Onoue T., Nakamura T., Haranosono T. and Yasuda C. (2011) Composition and accretion rate of fossil micrometeorites recovered in middle Triassic deep-sea deposits. *Geology* **39**, 567–570.

Parashar K., Prasad M. S. and Chauhan S. S. S. (2010) Investigations on a large collection of cosmic dust from the central Indian ocean. *Earth Moon Planets* **107**, 197–217.

Raghavan V. (2010) Fe_Ni-O (Iron-Nickel-Oxygen). *JPEDAV* **31**, 369–371.

Robin E., Jehanno C., and Maurette M. (1988) Characteristics and origin of Greenland Fe/Ni cosmic grains. 18th Lunar and Planetary Science Conference, Houston. P 593–598.

Rochette P., Folco L., Suavet C., van Ginneken M., Gattacceca J., Perchiazzi N., Braucher R. and Harvey R. P. (2008) Micrometeorites from the transantarctic mountains. *Proc. Natl. Acad. Sci.* **105**, 18206–18211.

Rowan C. J., Roberts A. P. and Broadbent T. (2009) Reductive diagenesis, magnetite dissolution, greigite growth and paleomagnetic smoothing in marine sediments: a new view. *Earth Planet. Sci. Lett.* **277**, 223–235.

Rudraswami N. G., Parashar K. and Prasad M. S. (2011) Micrometer- and nanometer-sized platinum group nuggets in micrometeorites from deep-sea sediments of the Indian Ocean. *Meteorit. Planet. Sci.* **46**, 470–491.

Rudraswami N. G., Prasad M. S., Plane J. M. C., Berg T., Feng W. and Balgar S. (2014) Refractory metal nuggets in different types of cosmic spherules. *Geochim. Cosmochim. Acta* **131**, 247–266.

Sauvet C., Gattacceca J., Rochette P. and Folco L. (2011) Constraining the terrestrial age of micrometeorites using their record of the Earth's magnetic field polarity. *Geology* **39**, 123–126.

Searle E. J. (1958) A note on the formation of native iron and other effects associated with contact of basalt and carbonized wood at Auckland, New Zealand. *New Zealand J. Geol. Geophys.* **1**, 451–458.

Sharan A. and Cramb A. W. (1997) Surface tension and wettability studies of liquid Fe-Ni-O alloys. *Metallurg. Mater. Trans. B* **28**, 465–472.

Shibata Y. (1996) Opaque minerals in Antarctic CO_3 carbonaceous chondrites, Yamato-74135, -790992, -791717, -81020, -81025, -82059 and Allan Hills-77307. *Proc. NIPR Symp. Antarct. Meteorit* **9**, 79–96.

Suk D., Peacor D. R. and Van der Voo R. (1990) Replacement of pyrite framboids by magnetite in limestone and implications for palaeomagnetism. *Nature* **345**, 611–613.

Taylor S. and Brownlee D. E. (1991) Cosmic spherules in the geologic record. *Meteoritics* **26**, 203–211.

Taylor S., Lever J. H. and Harvey R. P. (2000) Numbers, types and compositions of an unbiased collection of cosmic spherules. *Meteorit. Planet. Sci.* **55**, 651–666.

Taylor S., Jones K. W., Herzog G. F. and Hornig C. E. (2011) Tomography: a window on the role of sulfur in the structure of micrometeorites. *Meteorit. Planet. Sci.* **46**, 1498–1509.

Tepesch P. D. and Quong A. A. (2000) First-principle calculations of alpha-alumina (0001) surface energies with and without hydrogen. *Phys. Status Solidi B* **217**, 377–387.

Tomkins A. G., Mare E. R. and Raveggi M. (2013) Fe-carbide and Fe-sulfide immiscibility in IAB meteorite, Campo del Cielo: implications for iron meteorite chemistry and planetesimal core compositions. *Geochim. Cosmochim. Acta* **117**, 80–98.

Tomkins A. G., Bowlt L., Genge M., Wilson S. A. and Brand H. E. A. (2016) Ancient fossil micrometeorites suggestive of an oxygenated Archaean upper atmosphere. *Nature* **533**, 235–238.

Van Ginneken M., Folco L., Perchiazzi N., Rochette P. and Bland P. (2010) Meteoritic ablation debris from the Transantarctic Mountains: evidence for a Tunguska-like impact over Antartica ca. 480ka ago. *Earth Planet. Sci. Lett.* **293**, 104–113.

Van Ginneken M., Genge M. J., Folco L. and Harvey R. P. (2016) The weathering of micrometeorites from the Transantarctic Mountains. *Geochim. Cosmochim. Acta* **179**, 1–31.

Ubbelohde A. R. (1978) *Molten State of Matter: Melting and Crystal Structure*. Wiley-Blackwell.

Voldman G. G., Genge M. J., Albanesi G. L., Barnes C. R. and Ortega G. (2013) Cosmic spherules from the Ordovician of Argentina. *Geol. J.* **48**, 222–235.

West G. D., Birosca S. and Higginson R. L. (2005) Phase determination and microstructure of oxide scales formed on steel on high temperature. *J. Microscopy* **217**, 122–129.

Yada T., Nakamura T., Sekiya M. and Takaoka N. (1996) Formation process of magnetic spherules collected from deep-sea sediments – observations and numerical simulations of their

orbital evolution. *Proc. NIPR Symp. Antarct. Meteorites* **9**, 218–236.

Yiou F., Raisbeck G. M. and Brownlee D. E. (1985) 10Be in iron type cosmic spherules: evidence for a differentiated parent body. *Meteoritics* **20**, 791–792.

Young D. J. (2008) *High Temperature Oxidation and Corrosion of Metals*. Elsevier, Amsterdam, pp. 81–135.

Zhou W., Van Der Voo R., Peacor D. R., Wang D. and Zhang Y. (2001) Low-temperature oxidation in MORB titanomagnetite to titanomaghemite: a gradual process with implications for marine magnetic anomaly amplitudes. *J. Geophys. Res* **106**, 6409–6421.

Associate editor: Gregory F. Herzog